Lab on a Chip

CRITICAL REVIEW

View Article Online
View Journal | View Issue

Cite this: *Lab Chip*, 2026, **26**, 1588

Lymphatics-on-a-chip microphysiological system: engineering lymphatic structure and function *in vitro*

Yansong Peng and Esak Lee *

The lymphatic system—integral to fluid balance, immune surveillance, and lipid absorption—is frequently overlooked despite its vital roles. Traditional research modalities, including static two-dimensional cultures and animal models, have illuminated key molecular and cellular features but fall short in recapitulating human lymphatic function, due to limited physiological relevance, throughput, and mechanobiological complexity. Recent advances in microfluidic organ-on-a-chip systems offer biomimetic platforms that integrate three-dimensional architecture, fluid flow, and biomechanical stimuli alongside human lymphatic endothelial and supporting cells. These lymphatics-on-a-chip constructs faithfully reproduce dynamic behaviors such as fluid drainage, junction remodeling, and cell trafficking under physiological and pathological responses. This review highlights the foundational lymphatic biology and engineering principles behind these devices, their capacity for disease modeling and drug testing, and their potential to drive future innovation through induced pluripotent stem cell integration, organ-specific customization, and computational modeling. Merging bioengineering, cell biology, and machine learning, lymphatic microphysiological systems stand poised to significantly expand our understanding and treatment of lymphatic-related disorders.

Received 13th September 2025,
Accepted 30th November 2025

DOI: 10.1039/d5lc00875a

rsc.li/loc

1 Introduction

Lymphatic vessels play critical roles in maintaining fluid balance, transporting dietary fats, and orchestrating immune cell trafficking.[1,2] Unlike the blood vasculature, which historically received more attention, the lymphatic system's roles in health and disease have only recently come to the fore. Indeed, an NIH workshop in 2022 highlighted lymphatics as "yet to be charted" and identified critical gaps in our understanding of lymphatic development, function, and pathology.[2] These thin-walled vessels were once viewed mainly as passive drains, but modern research reveals them as active regulators at the interface of tissue homeostasis, immune surveillance, and disease progression.[3,4] It is now recognized that lymphatic dysfunction underlies a broad spectrum of diseases beyond classical lymphedema—including autoimmune diseases,[5–9] obesity,[10–14] cardiovascular diseases,[15–17] neurological disorders,[18–20] and cancer.[21,22]

Existing experimental models for lymphatic biology include traditional two-dimensional (2D) LEC monolayers and *in vivo* animal systems such as mouse or zebrafish models. While these platforms have revealed many aspects of lymphatic development and physiology, they each carry limitations: 2D cultures lack vessel-level architecture, fluid flow, and matrix anchoring; animal models, though physiologically complete, are species-specific, lower-throughput, and less amenable to mechanical or biochemical control. These limitations motivate the development of organ-on-a-chip models of the lymphatic system, which can recapitulate the unique structure and biomechanical context of lymphatic vessels *in vitro*.[23] Traditional cell culture often falls short in capturing the biophysical environment and discontinuous cell–cell junctions characteristic of lymphatics. By leveraging microfluidic technology and biomaterials, lymphatics-on-a-chip platforms aim to provide more physiologically relevant models for basic research and translational applications. Such systems offer precise control over fluid flow, pressure, and biochemical gradients, enabling researchers to probe lymphatic functions under well-defined conditions.[24] Moreover, integrating lymphatic vessels on chip with other tissue compartments or immune components opens new avenues to study interstitial transport, immunology, and cancer metastasis in a controlled setting. Ultimately, lymphatic microphysiological models are poised to accelerate the discovery of lymphatic-specific therapeutics and personalized medicine approaches for lymphatic-related pathologies.

This review provides a comprehensive overview of the emerging field of lymphatics-on-a-chip. We first summarize

Nancy E. and Peter C. Meinig School of Biomedical Engineering, Cornell University, Ithaca, NY 14853, USA. E-mail: el767@cornell.edu

foundational principles of lymphatic biology (*i.e.*, developmental origins, unique structural features, and mechanobiological hallmarks). We then discuss microfluidic and biomimetic engineering strategies to model lymphatics *in vitro*, including device designs, biomaterials, and flow control. Next, we survey applications of lymphatic chips in modeling diseases such as lymphedema, cancer, autoimmune diseases, and neurological disorders. Finally, we outline future directions, including induced pluripotent stem cell (iPSC)-derived lymphatic organoids, multi-scale coupling of lymphatics with other organ systems, and AI-driven design and analysis of lymphatic networks. In this review, we synthesize findings across studies to provide a cohesive understanding of how lymphatics-on-a-chip technology advances lymphatic research.

2 Foundational principles of lymphatic biology

Seminal discoveries over the past two decades have redefined our understanding of lymphatic biology. In the early 2000s, a series of studies demonstrated that tumors exploit lymphangiogenesis to facilitate metastasis: overexpression of vascular endothelial growth factor C/D (VEGF-C/D) in mouse models induced new lymphatic growth and increased tumor spread to lymph nodes.[25–28] Clinical data support this link in humans, showing that higher tumor-associated lymphatic vessel density (LVD) correlates with increased lymph node metastasis and poorer survival in solid tumors.[29–32] Blocking VEGF-C or vascular endothelial growth factor receptor 3 (VEGFR-3) could suppress lymphatic metastasis in mice, establishing these pathways as promising therapeutic targets. Such findings, along with the cloning of prospero homeobox 1 (PROX1) and identifying the first lymphatic-specific markers—LYVE-1, podoplanin (PDPN), and VEGFR-3 (FLT4)—enabled definitive discrimination between lymphatic and blood endothelial cells. These breakthroughs transformed lymphatic research from descriptive anatomy to molecular and functional biology, paving the way for mechanistic and engineering studies. Lymphatics-on-a-chip technology arises from this foundation, aiming to integrate these molecular pathways and cellular behaviors into microengineered platforms that enable controlled, quantitative exploration of lymphatic development, transport, and disease.

2.1 Developmental origins and tissue-specific heterogeneity of lymphatic vessels

Lymphatic endothelial cells (LECs) share core endothelial markers such as VE-cadherin and CD31, yet express distinct molecules including LYVE-1, podoplanin, and the transcription factor PROX1, which together define lymphatic identity.[33] Classical studies established that mammalian lymphatics arise primarily from PROX1$^+$ endothelial cells sprouting from the cardinal veins.[28] More recent lineage-tracing and single-cell analyses, however, reveal additional non-venous sources, including mesenchymal angioblasts in the dermomyotome, mesentery, heart, and kidney, that differentiate directly into LECs through VEGF-C/VEGFR-3 and SOX18/COUP-TFII signaling.[33] These findings support a model in which lymphatic vasculogenesis complements venous lymphangiogenesis, contributing to regional diversity. Regardless of origin, PROX1 acts as the master regulator of LEC fate, activating downstream genes (VEGFR-3, LYVE-1, podoplanin) and suppressing the blood endothelial program.[34] In mice, loss of Prox1 abolishes lymphatic formation, while mutations in VEGF-C/VEGFR-3 cause primary lymphedema in humans.[3,35]

Recognizing this developmental heterogeneity is important for organ-specific lymphatic modeling on chip, where different progenitor programs and signaling environments may need to be recapitulated to mimic lymphatics across tissues.[36] For example, dermal lymphatics form dense, blind-ended capillary networks with permeable button-like junctions that facilitate immune cell trafficking and interstitial fluid drainage.[37] Intestinal lacteals located within villi, on the other hand, exhibit dynamic zipper-to-button transitions during lipid absorption, a process tightly regulated by VEGF-A/VEGFR-2 and Notch signaling.[38,39] Meningeal lymphatics, which develop postnatally along the dural sinuses and skull base, connect to deep cervical lymph nodes and the glymphatic pathway to drain cerebrospinal fluid and metabolic waste from the brain, linking the central nervous system to systemic immunity.[40,41] These diverse architectures underscore how developmental origin and local microenvironment shape lymphatic structure and function. Reproducing such regional diversity, through appropriate matrix stiffness, junctional morphology, and flow regimes, is central to engineering organ-specific lymphatics-on-a-chip that accurately model physiological and pathological lymphatic functions.

2.2 Architectural and functional specialization of lymphatic vessels

The lymphatic vasculature forms a one-way transport network that drains interstitial fluid and cells from tissues back into the blood circulation (Fig. 1).[3] The system begins with blind-ended initial lymphatic capillaries, which are composed of a single layer of oak leaf-shaped LECs connected by discontinuous, "button-like" junctions.[42,43] These button junctions and overlapping endothelial flaps act as primary valves that allow fluid and immune cell entry from the interstitium.[43] Anchoring filaments tether LECs to the extracellular matrix; when interstitial pressure rises, the filaments pull the flaps open, thereby enhancing fluid uptake.[3] As these capillaries converge into larger collecting lymphatic vessels, the endothelial junctions transition to continuous "zipper-like" junctions, with fewer gaps that reduce permeability.[3,42] Collecting lymphatics also feature intraluminal valves and are ensheathed by lymphatic muscle cells (LMCs), which generate rhythmic contractions to propel

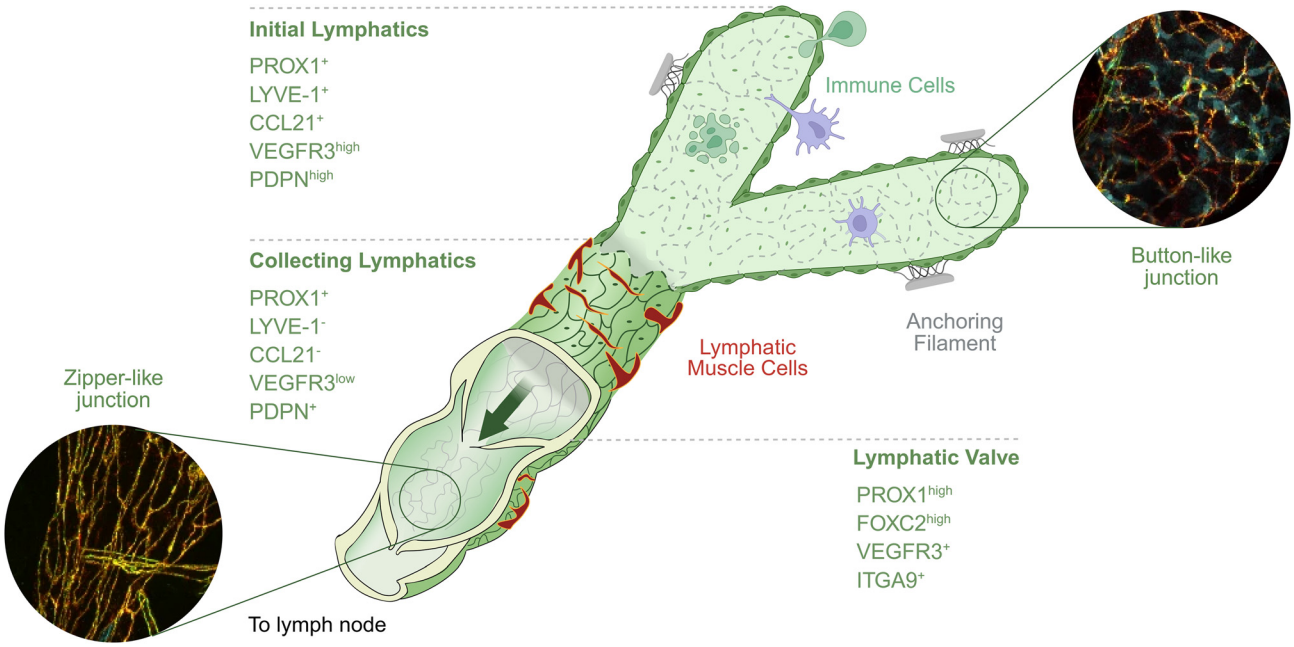

Fig. 1 Architectural organization and molecular signatures of lymphatic vessels. The lymphatic vasculature is organized into blind-ended initial lymphatic capillaries, transitional pre-collecting vessels, and contractile collecting lymphatic vessels with intraluminal valves. Initial lymphatics consist of oak leaf-shaped LECs connected by discontinuous button-like junctions (blue: LYVE-1; red: VE-cad) that permit uptake of interstitial fluid, macromolecules, lipids, and immune cells. Anchoring filaments tether LECs to the extracellular matrix, enabling pressure-driven flap opening. Pre-collecting and collecting vessels progressively acquire continuous zipper-like junctions (blue: LYVE-1; red: VE-cad), basement membrane, smooth muscle coverage, and valves that maintain unidirectional flow. Marker expression distinguishes vessel compartments: LYVE-1, VEGFR3, and CCL21 highlight initial lymphatics, while FOXC2 and integrin-α9 are enriched in collecting vessels and valve-forming LECs. This compartmentalization underlies the dual role of lymphatics in tissue fluid absorption and long-distance lymph transport. Adapted with permission from Yijie Hua. Inset panels adapted with permission from ref. 47, copyright 2025 Springer Nature. Created with https://BioRender.com.

lymph forward. This hierarchical organization ensures efficient absorption from tissues and unidirectional transport through lymph nodes—where immune filtering occurs—before lymph empties into the subclavian veins.[3]

This structural design underpins the diverse physiological functions of the lymphatic system. First, lymphatics serve as the body's fluid homeostasis system, continuously returning plasma ultrafiltrate that leaks from blood capillaries. In humans, this amounts to an estimated ~2–4 liters of fluid per day being returned to the venous circulation under steady-state conditions, preventing edema.[1,44] Second, lymphatics provide a specialized route for lipid absorption. In the intestine, lacteals (*i.e.*, specialized lymphatic capillaries in the villi) absorb chylomicrons (*i.e.*, dietary lipid-laden lipoproteins) and transport them *via* the thoracic duct to the bloodstream.[14] In addition, recent studies highlight a role for lymphatics in cholesterol clearance, where interstitial high-density lipoproteins (HDLs) are ferried back to the circulation, reducing atherosclerotic risk.[15]

Beyond fluid and lipid transport, lymphatic vessels are increasingly recognized as active players in immunity. LECs constitutively secrete CC chemokine ligand 21 (CCL21), which guides CC Chemokine receptor 7-positive ($CCR7^+$) immune cells, including dendritic cells and T cells, into initial lymphatics through button junction gaps.[45] Antigens, cytokines, and immune cells entering lymphatics are carried to lymph nodes, where adaptive immune responses are initiated. Moreover, LECs themselves can regulate immunity: they can present antigens directly, modulate their access to lymph nodes, or express checkpoint molecules (*e.g.*, programmed death-ligand 1 (PD-L1)) that influence T-cell activation and tolerance.[4,46] Thus, lymphatic vessels are far more than passive conduits—they actively coordinate immune surveillance, tolerance, and inflammation.

2.3 Mechanobiological regulation of lymphatic junctions and valve development

Lymphatic vessels are exquisitely sensitive to mechanical forces within their environment. Fluid shear stress from lymph flow, cyclic stretch caused by vessel pumping, and matrix tethering forces collectively shape LEC phenotypes (Fig. 2). A key outcome of these stimuli is the regulation of intercellular junctions in initial lymphatics, which control permeability and determine whether vessels adopt specialized button- or zipper-like configurations, as well as valvulogenesis in collecting lymphatics, which guide the unidirectional lymph flow. Understanding these mechanobiological mechanisms is essential to decipher how lymphatics maintain homeostasis and how perturbations such as inflammation, hypertension, or exercise drive lymphatic remodeling or dysfunction.

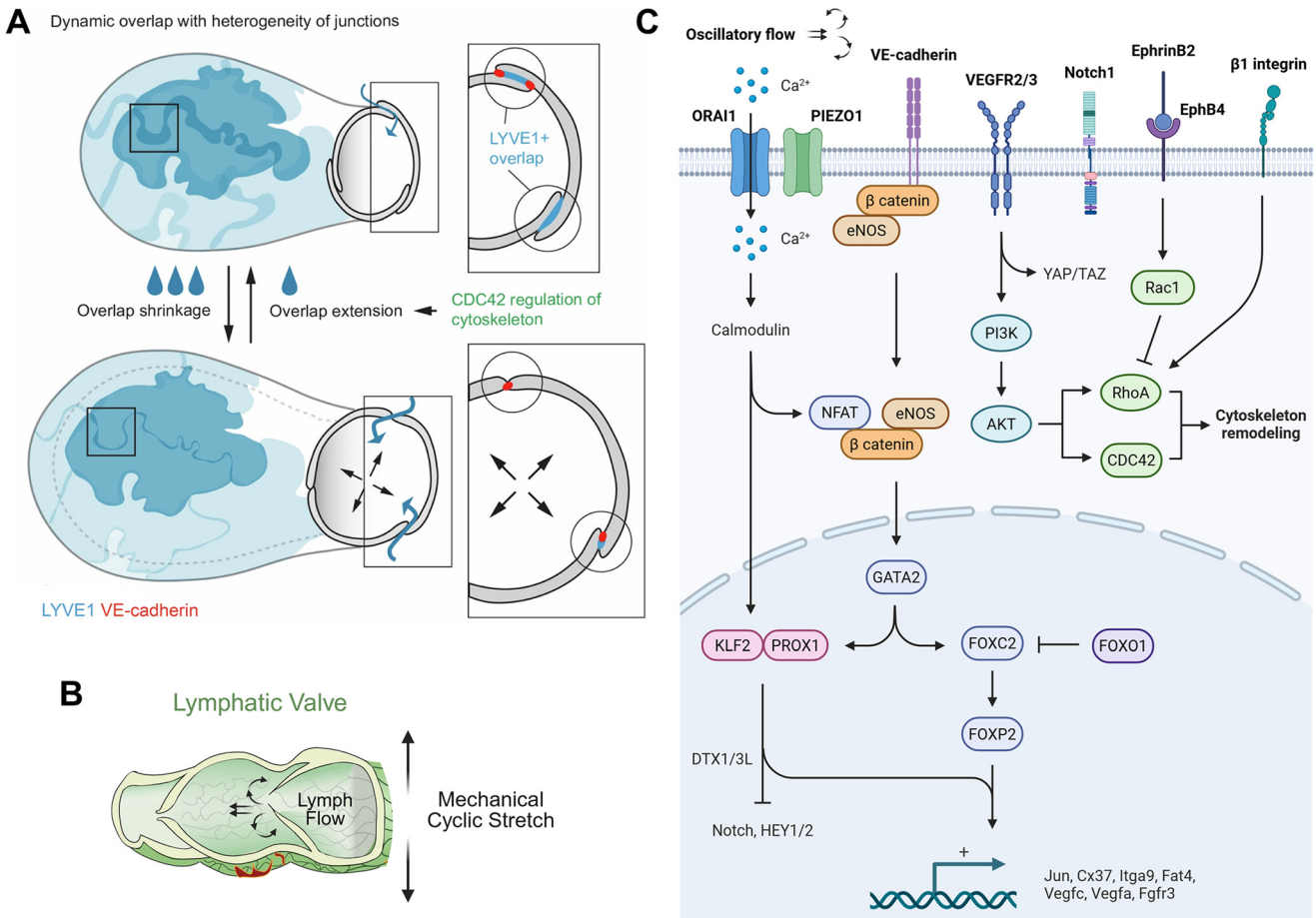

Fig. 2 Mechanobiological regulation of lymphatic junction dynamics, shear sensing, and valve development. (A) Proposed model of lymphatic capillary function driven by dynamic remodeling of LEC overlaps. Puzzle-shaped capillary LECs exhibit LYVE1$^+$ cellular overlaps with diverse junctional configurations. Increased interstitial fluid shortens overlaps to permit lumen expansion during uptake, countered by CDC42-mediated actin remodeling that extends lamellipodia-like overlaps to maintain monolayer integrity and barrier strength. This supports a bellows-like mechanism in which overlap extension compresses the vessel and aids fluid propulsion. Adapted with permission from ref. 47, copyright 2025 Springer Nature. (B) Lymph flow maintains expression of mechanosensitive transcription factors FOXC2, GATA2, and NFATc1 and preserves collecting vessel and valve function. Adapted with permission from ref. 40, copyright 2020 American Association for the Advancement of Science. (C) Mechanosensory pathways regulating junction remodeling and valve specification. LECs sense shear stress through a junctional mechanosensory complex (VE-cadherin, VEGFR2, VEGFR3) that activates PI3K-Akt, cytoskeletal remodeling, and YAP/TAZ signaling; and the stretch-activated ion channel PIEZO1, which engages the calcium channel ORAI1. The resulting calcium influx activates calmodulin, which complexes with KLF2 to regulate transcriptional programs. Together, these pathways control key regulators of lymphatic identity and valve morphogenesis, including PROX1, FOXC2, GATA2, NFATc1, Cx37, integrin-α9, FAT4, and E3 ubiquitin ligases DTX1/3L. Adapted with permission from ref. 63, copyright 2023 Springer Nature. Created with https://BioRender.com.

2.3.1 Force-driven specialization and plasticity of lymphatic junctions. Lymphatic endothelial junctions display two characteristic organizational states—button-like junctions in initial lymphatic capillaries and zipper-like junctions in collecting vessels—each supporting distinct modes of barrier function and fluid transport. These patterns arise through developmental maturation, but they remain dynamically modifiable in adult tissues in response to mechanical, biochemical, and inflammatory cues.

Developmental specialization is reinforced by multiple signaling pathways that stabilize junction architecture. Jun proto-oncogene (Jun) and EphrinB2-EphB4 signaling provide tonic junctional control in lymphatic capillaries and collectors, respectively.[48,49] Fu *et al.* (2023) demonstrated that mechanical pressure at birth induces c-JUN expression in LECs, driving actin cytoskeletal remodeling that enables the opening of neonatal lung lymphatics; loss of c-JUN prevents vessel opening, causes fluid retention, and results in neonatal lethality.[48] Likewise, Frye *et al.* (2020) showed that disruption of EphrinB2-EphB4 signaling destabilizes VE-cadherin junctions, increases actomyosin contractility, and induces lymphatic leakage, effects not observed in blood vessels, while EphrinB2-Fc supplementation restores junctional integrity.[49]

Beyond developmental regulation, junctions in initial lymphatic capillaries exhibit pronounced mechanical plasticity. These vessels undergo continuous distension and recoil as they fill and empty. Schoofs *et al.* (2025) used

intravital microscopy and on-chip stretch assays to show that cyclic strain drives reversible changes in LEC overlap. During vessel expansion, overlapping flaps partially retract but are reinforced by Cell division control protein 42 homolog (CDC42)-dependent actin protrusions reminiscent of "puzzle-piece" plant cells. On-chip cyclic stretch (~12% strain at 0.01 Hz) reproduced these dynamics, whereas CDC42 inhibition yielded fragile, leaky junctions *in vivo* and *in vitro*. These observations support a "bellows" model in which LEC overlaps narrow during filling and re-expand during emptying, enabling a barrier that is both resilient and permissive to fluid entry (Fig. 2A).[47]

Junctional plasticity is also shaped by inflammatory and growth factor signaling. Cromer *et al.* (2014) reported that cytokines such as TNF-α, IL-6, IL-1β, and IFN-γ substantially increase LEC permeability, largely through nitric oxide-dependent VE-cadherin destabilization and actomyosin contraction.[50] With prolonged inflammation, these signals can drive reversible transitions between button-like and zipper-like configurations. Seminal work by Baluk *et al.* (2007) and Yao *et al.* (2012) demonstrated that button junctions in initial lymphatics can convert to zipper-like junctions, reducing fluid uptake capacity, but that dexamethasone treatment restores button prevalence, highlighting the reversibility of this process.[51,52]

Together, these findings indicate that lymphatic junction organization is defined by both developmental specialization and post-developmental plasticity, with mechanical forces and inflammatory cues acting synergistically to remodel junctions—often at the expense of drainage efficiency.

2.3.2 Oscillatory flow-dependent mechanotransduction in lymphatic valve formation. Collecting lymphatic vessels depend on intraluminal valves for unidirectional flow, and their development is tightly regulated by fluid flow-induced mechanotransduction (Fig. 2B). Genetic regulators such as PROX1, Forkhead box protein C2 (FOXC2), GATA-binding factor 2 (GATA2), integrin-α9, and VEGFR3 are enriched in valve-forming LECs, but their activation requires oscillatory flow.[53] In mice, valves first appear in mesenteric lymphatics shortly after lymph flow begins (E15.5), where oscillatory shear at vessel branch points induces nuclear β-catenin and upregulation of PROX1 and FOXC2, marking clusters of valve progenitors.[54] PROX1 and FOXC2 constitute a core transcriptional module: FOXC2-deficient mice completely lack valves and develop lymphedema-distichiasis, underscoring their essential role.[55,56] Flow patterns critically shape this program. Choi *et al.* (2017) showed that steady laminar shear (~0.5–5 dyne per cm^2) induces KLF2 but does not activate valve-specific genes. By contrast, oscillatory shear (~1 dyne per cm^2) preferentially upregulates FOXC2, GATA2, and connexin37, key determinants of valve-forming identity. Prolonged high shear can even downregulate PROX1, reprogramming LECs toward a blood endothelial phenotype.[57] These findings establish oscillatory shear as the primary mechanical cue driving valve specification. Downstream, PROX1 and FOXC2 cooperate with shear-responsive pathways to execute morphogenesis. Sabine *et al.* (2012) identified connexin37 as a direct target of PROX1/FOXC2 under shear, required for valve cell communication and leaflet assembly.[56] They also linked shear to calcineurin/NFAT activation, which synergizes with PROX1-FOXC2 to drive valve-specific gene expression; inhibition of calcineurin phenocopies FOXC2 loss, causing valve defects.[56] In addition, a recent study by Hernández-Vásquez *et al.* (2021) identified Forkhead box protein P2 (FOXP2) as a new flow-induced transcriptional regulator of lymphatic valve development downstream of FOXC2/NFATc1.[58] Mechanosensors translate these flow-induced shear forces into downstream signals. The stretch-activated ion channel PIEZO1 is indispensable: human PIEZO1 mutations cause congenital lymphedema, and endothelial PIEZO1 knockout mice develop rudimentary valves that fail to remodel despite initiating FOXC2 and NFAT expression. Pharmacological activation of PIEZO1 (*via* Yoda1) restores cytoskeletal remodeling and VE-cadherin dynamics, directly linking flow forces to valve morphogenesis.[59] Complementarily, endothelial nitric oxide synthase (eNOS) provides an NO-independent mechanosensory role. Iyer *et al.* (2023) showed that loss of eNOS reduces valve progenitor clusters by ~45%, due to impaired β-catenin stabilization and nuclear translocation under oscillatory shear. Rescue by Forkhead box protein O1 (FOXO1) deletion highlighted eNOS as a scaffold linking shear to β-catenin activation and FOXC2 expression.[54] Taken together, valve development integrates oscillatory shear, calcium influx (PIEZO1, ORAI1), β-catenin, NFAT, and core transcription factors (PROX1, FOXC2, GATA2) into a coordinated program that specifies valve cells, drives collective migration, and assembles functional bileaflet structures (Fig. 2C). Defects in this mechanotransduction network underlie congenital lymphedema syndromes, while persistent PIEZO1 activity in adulthood remains critical for valve stability and broader lymphatic function.[60]

2.3.3 Shear-activated lymphatic endothelial remodeling. LECs are highly mechanosensitive, expressing receptors such as VEGFR3 and β1 integrins at higher levels than blood endothelial cells (BECs).[61,62] Even minute pressure gradients (*i.e.*, on the order of millimeters of mercury (mmHg)) drive interstitial fluid into initial lymphatics, producing very low interstitial flow speeds (~0.1–1 μm s^{-1}) and shear stresses (~0.1–2 dyne per cm^2). By contrast, collecting lymphatics experience pulsatile flows generated by intrinsic contractions and skeletal muscle activity, with average shear around 1–2 dyne per cm^2 but transient spikes reaching 10–12 dyne per cm^2 during valve opening. Under pathological conditions such as lymphedema, abnormal collateral vessels have been reported to experience shear stresses up to 40 dyne per cm^2, underscoring the importance of flow regulation.[63] Pioneering work by Bonvin *et al.* (2010) showed that LECs aligned with interstitial flow and exhibited network-like structures, suggesting that mechanical forces plus stromal signals regulate lymphatic morphogenesis.[64] More recently, Choi *et al.* (2017) demonstrated that shear stress triggers distinct

responses in LECs *versus* BECs. Under steady shear (~2 dyne per cm^2), both cell types elongated and upregulated Kruppel-like factor 2 (KLF2). However, only LECs showed Notch pathway downregulation: shear exposure reduced NOTCH1 intracellular domain (NICD) levels and decreased expression of target genes Hairy/enhancer-of-split related with YRPW motif 1 (HEY1) and HEY2.[57] Mechanistically, shear-induced calcium influx *via* ORAI calcium release-activated calcium modulator 1 (ORAI1) activated calmodulin and promoted the formation of a PROX1-KLF2 transcriptional complex. This complex induced ubiquitin ligases Deltex E3 ubiquitin ligase 1/3L (DTX1/3L), which targeted NOTCH1 for degradation (Fig. 2C).[65] The outcome was enhanced sprouting capacity, consistent with *in vivo* findings that KLF2 deletion impairs lymphatic growth and causes edema. In contrast to blood vessels—where shear stabilizes vessels by upregulating Notch—lymphatic shear selectively tunes down Notch, promoting adaptive expansion.

Mechanobiology studies collectively demonstrate that lymphatic junctions are dynamic, mechano-responsive structures. Shear stress activates PROX1–KLF2 pathways to downregulate Notch and promote sprouting, stretch engages CDC42-driven actin remodeling to preserve junctional overlap, and inflammatory cues synergize with mechanical load to remodel button/zipper junctions. At valves, piezo1 and FOXC2 translate oscillatory flow into structural stability. These insights highlight multiple druggable targets to modulate lymphatic function and underscore the value of lymphatics-on-a-chip platforms for applying controlled mechanical environments. By bridging *in vivo* observations with tunable microengineered models, the field is now positioned to dissect mechanotransduction pathways with unprecedented precision. Table 1 summarizes some key physiological values in establishing lymphatic vasculature. It is important to emphasize that most of the available data derives from animal or *ex vivo* systems. Quantitative, *in vivo* measurements in human lymphatic vessels remain extremely limited, so translation to human-on-a-chip models should rely on dimensionless analysis and scaling rather than assuming direct equivalence. Future work is required to establish normative values in human lymphatics and validate mechanobiological findings in human-relevant systems.

Table 1 Representative physiological parameters governing lymphatic mechanics, transport, and flow regulation

Parameter	*In vivo* values	Species/tissues	Ref.
Interstitial fluid pressure	Subatmospheric (−1 to −3 mmHg) in loose tissues	Various species and tissues	66–68
Interstitial fluid flow velocity	0.1 to 1.0 μm s^{-1}	Rabbit dermis	69, 70
Hydraulic pressure (initial lymphatics)	Similar to interstitial pressure (−6 to 4 mmHg)	Rabbit and rat diaphragm, cat mesentery	71–74
Hydraulic pressure (collecting lymphatics)	5 to 10 cmH_2O (4 to 7 mmHg) diastolic pressure during relaxation	Rat mesentery	75, 76
Interstitial colloid osmotic pressure	8 to 17 mmHg	Human and pig various tissues	77, 78
Lymphatic colloid osmotic pressure	5 to 15 mmHg	Rat tail and dog hindleg prenodal lymph	79, 80
Lymph flow velocity (initial lymphatics)	0 to 29 μm s^{-1}	Mouse and human dermal tissues	81, 82
Lymph flow velocity (collecting lymphatics)	40 to 70 μm s^{-1} in mouse; 0.7 to 1 mm s^{-1} in rat; up to 9 mm s^{-1} during phasic contractions in rat	Mouse hindlimb, rat mesentery	83, 84
Volumetric lymph flow rate (single vessel)	0.5 to 2.5 μL h^{-1} in mouse; 9 to 19 μL h^{-1} in rat	Mouse hindlimb, rat mesentery	83, 84
Volumetric lymph flow rate (under stress)	Increases ~6× under acute fluid load: ~0.1 μL min^{-1} baseline to ~0.6 μL min^{-1}	Rat mesentery (acute edema state)	85
Total lymph flow (whole body)	3 to 4 L per day in an average adult at rest; can increase several-fold with exercise	Pig thoracic duct output	86
Wall shear stress (initial lymphatics)	Extremely low, 0.01 to 0.06 dyne per cm^2	Mouse dermis	87, 88
Wall shear stress (collecting lymphatics)	0.5 to 0.8 dyne per cm^2 during steady flow; pulsatile peaks 4 to 12 dyne per cm^2 due to lymphatic contractions	Rat mesentery	83
Wall shear stress (edema)	Time averaged 1.5 dyne per cm^2; 5 to 40 dyne per cm^2 during strong flow pulses	Rat mesentery (acute edema state)	85
Intrinsic pumping frequency	0.08 to 0.27 Hz (5 to 19 contractions per minute)	Rat various tissues	89, 90
Maximal pumping pressure (occlusion pressure)	80 to 100 mmHg	Human dermis	91
Lymphatic junction overlap (buttons)	0.5 to 3.5 μm (width per flap); 70 to 175 $μm^2$ (area between flaps)	Mouse ear and trachea	47, 51
Lymphatic capillary diameter	30 to 70 μm	Rat mesentery and human dermis	82, 92
Lymphatic collector diameter	60 to 120 μm	Rat mesentery	89, 93, 94
Hydraulic conductivity	17.3×10^{-7} cm s^{-1} cmH_2O^{-1}	Mouse mesentery	95

3 Microfluidic and biomimetic engineering strategies for lymphatic systems

Early efforts in this field have drawn inspiration from well-established blood vessel-on-chip models, adapting them to the unique features of lymphatics.[96,97] However, lymphatic vessels differ from blood vessels in essential ways, including their developmental origins, ultrastructure (*e.g.*, specialized cell–cell junctions and valves), lower shear stress environments, and function as unidirectional absorbent conduits.[1,98] Over the past decade, researchers have made significant strides in capturing these distinctions (Fig. 3), including (1) engineering lymphatic capillary networks *in vitro via* lymphangiogenesis[99–101] (*i.e.*, sprouting from pre-existing vessels) or vasculogenesis[102–105] (*i.e.*, self-assembly from dispersed cells); (2) reproducing lymphatic vessel structure[106–110]—notably the unique discontinuous "button-like" junctions of initial lymphatics and mural cell coverage of collecting lymphatics; and (3) applying biomechanical forces (*e.g.*, interstitial flow, shear, stretch) to mimic lymphatic fluid dynamics.[108,111–113]

3.1 Lymphangiogenesis-based engineering of perfusable lymphatic capillaries

Noo Li Jeon and colleagues pioneered a biomimetic lymphangiogenesis-on-chip model that closely mimics *in vivo* sprouting. Kim *et al.* (2016)[99] described a 3D microfluidic platform integrating key elements of the lymphatic niche—biochemical gradients, interstitial flow, and stromal cell interactions—to induce robust sprouting of LECs into a fibrin matrix (Fig. 3A). In their device, a lumen lined by LECs was formed adjacent to a tissue chamber containing fibroblasts, with a gradient of pro-lymphangiogenic factors (*e.g.*, VEGF-C) established across the matrix. Under these conditions, LECs sprouted from the vessel and invaded the matrix, forming multicellular capillary projections. Notably, a slow interstitial flow was applied from the tissue side toward the lymphatic channel to emulate fluid drainage. This interstitial flow proved a crucial regulator: it significantly enhanced the initiation and directional bias of lymphatic sprouting. LEC sprouts preferentially extended upstream against the flow, consistent with how tissue fluid flow *in vivo* can guide lymphangiogenesis towards the source of drainage. With the right synergy of flow and growth factors, the *in vitro* sprouts displayed hallmarks of native lymphatic vessels, including migratory tip cells and lumen formation, and responded appropriately to pro- and anti-lymphatic stimuli. This model demonstrated for the first time the feasibility of reconstituting sprouting lymphangiogenesis *in vitro* in a controlled manner, highlighting that a combination of VEGF-C and interstitial flow is key to inducing robust, directional lymphatic sprouting.[99] Osaki *et al.* (2018)[100] extended this synergy concept to a dual vascular model (Fig. 3B). Using sacrificial molding, they created a microdevice embedding both lymphatic vessels and blood vessels—600 μm channels seeded with human LECs and HUVECs, respectively—and induced angiogenesis and lymphangiogenesis *via* perfusion combined with VEGF-A or VEGF-C and phorbol 12-myristate 13-acetate (PMA). Remarkably, they observed that vascular angiogenesis facilitated lymphatic sprouting through local matrix metalloproteinase (MMP) secretion by endothelial cells. Specifically, a VEGFR-3 inhibitor blocked lymphangiogenesis in the absence of BVs, but not when BVs were present, indicating that blood-vascular-derived MMPs can compensate for lymphatic angiogenic signaling—highlighting crosstalk between the two vascular beds.[100] Building on this, Jain and colleagues (2024) recently reported a lymphangiogenesis-on-chip system examining the independent and combined effects of biochemical gradients and interstitial flow. In their study, LECs were subjected to varying conditions: VEGF-C gradients alone, interstitial flow alone, or both together. They found that each factor could stimulate some degree of sprouting, but the combination produced the most extensive and physiologically oriented networks (with flow directing the sprouts).[101] This confirms a synergistic paradigm: slow steady flow (~1–5 μm s^{-1}) synergizes with VEGF-C signaling to amplify lymphatic sprouting and helps define the polarity of growth (*i.e.*, which way sprouts grow). Mechanistically, interstitial flow appears to increase the availability and cell uptake of matrix-bound VEGF-C, as well as to upregulate LEC responsiveness to growth factors. Moreover, flow can work in concert with other biochemical cues; for example, gradients of sphingosine-1-phosphate (S1P)—absent in interstitium but present in lymph—were shown to cooperate with flow in guiding LEC migration and sprouting.[63,101] These findings underscore that engineered lymphatic sprouting requires orchestrating multiple biochemical and biophysical cues, much like during developmental lymphangiogenesis.

3.2 Matrix and scaffold engineering for lymphatic vasculogenesis

The choice of extracellular matrix (ECM) environment is another critical design parameter. LECs generally require a 3D matrix (*e.g.*, collagen or fibrin) to form tubular structures. Matrix stiffness, porosity, and adhesive ligand composition all influence lymphatic morphogenesis.[114,115] Hanjaya-Putra's group has conducted detailed studies on how matrix stiffness "primes" lymphatic capillary formation. In a 2D culture, they observed that softer substrates promoted LEC elongation and sprout-like behavior in response to VEGF-C, whereas stiffer substrates did not—hinting that compliance might be necessary.[116] They then moved to 3D hydrogels: Alderfer *et al.* (2021) showed that a relatively soft hydrogel (with shear modulus on the order of a few hundred Pascals) was optimal for LEC tube formation when VEGF-C was provided, whereas higher stiffness (>1 kPa) markedly impaired sprouting.[116] In a follow-up study, Alderfer *et al.* (2024) developed a synthetic modular

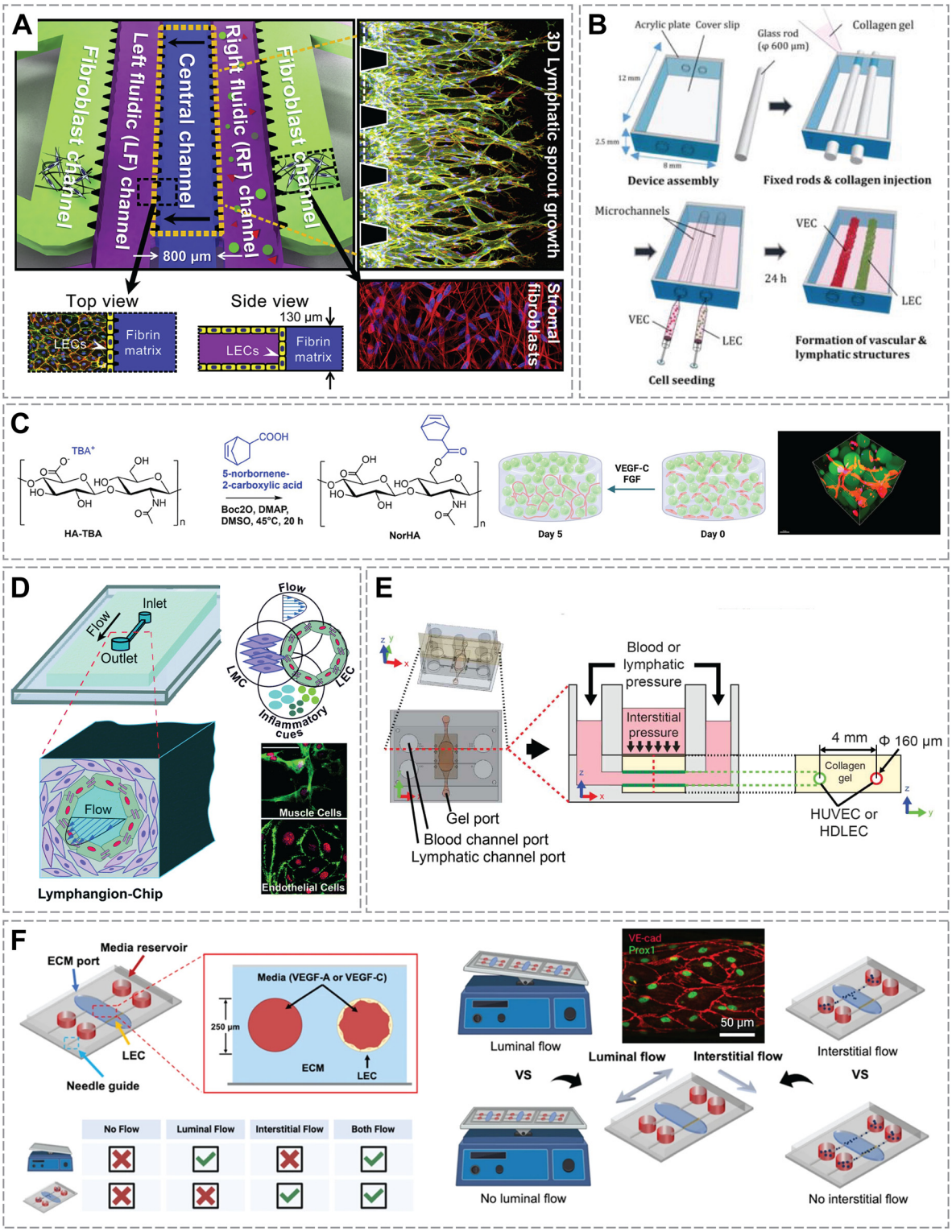

Fig. 3 Microfluidic and biomimetic engineering strategies for reconstituting lymphatic structure and function *in vitro*. (A) Microfluidic device for reconstitution of 3D sprouting lymphangiogenesis *in vitro*. Adapted with permission from ref. 99, copyright 2016 Elsevier. (B) Schematic illustration and fabrication process of engineered lymphatic and vascular structures to study cooperative effects of vascular angiogenesis and lymphangiogenesis. Adapted with permission from ref. 100, copyright 2018 Springer Nature. (C) Graphical representation of granular hydrogel composites fabrication and lymphatic sprouting assays, with 3D rendering of V180s gel (green—FITC) exhibiting lymphatic capillary network formation (red—F-actin). Adapted with permission from ref. 105, copyright 2025 Wiley-VCH. (D) An engineering drawing of the lymphangion-chip and a representative confocal image set of on-chip LMCs (green: F-actin) and LECs (green: VE-cadherin) under co-culture conditions. Scale bar: 50 μm. Adapted with permission from ref. 107, copyright 2022 Royal Society of Chemistry. (E) Mμlti-flow platform design and device structure. Adapted with permission from ref. 112, copyright 2022 IOP Publishing. (F) An engineered 3D lymphatic vessel-on-chip model to investigate luminal and interstitial flow effects with VEGF-A or VEGF-C. Adapted with permission from ref. 108, copyright 2023 Springer Nature.

hydrogel (*i.e.*, norbornene-functionalized hyaluronic acid) where they could tune stiffness and integrin-binding content independently. They found that a mid-range stiffness (~500 Pa), including fibronectin-mimetic RGD peptides, yielded robust formation of lumenized lymphatic capillaries in 3D. Softer gels (~100 Pa) allowed initial capillary assembly but were too weak to support network stability beyond a few days, while stiffer gels (~1–2 kPa) completely inhibited LEC elongation into tubes. Interestingly, LECs in the stiff hydrogels upregulated matrix-degrading enzymes (MMP-2, MMP-14) and VEGFR3 expression, as if attempting to compensate for the non-permissive environment. However, no stable tubes were formed in the stiff condition even over 3 weeks.[104] These results indicate that matrix mechanics can control lymphatic morphogenesis: a compliant matrix "primes" LECs to respond to VEGF-C by forming cords or tubes, whereas a rigid matrix triggers a phenotypic response (*i.e.*, upregulating proteases and VEGFR3) but prevents actual sprout penetration. From an engineering perspective, tuning scaffold stiffness is essential for building lymphatic networks on-chip. It also suggests that the *in vivo* fibrotic or tumor stroma (often stiffer than healthy tissues) might inherently resist lymphangiogenesis. Adhesive cues are another factor required for LECs to form 3D structures. Alderfer *et al.* (2024) showed that adding an RGD peptide (which binds integrins α5β1 and αvβ3) to a hydrogel markedly improved LEC sprouting and branch formation. Without RGD, LECs remained mostly round in 3D culture; with an optimal concentration (~5 mM) of RGD, they formed extensive tube networks. This mirrors earlier observations that fibronectin (an RGD-containing ECM protein) promotes lymphatic endothelial proliferation and tube formation. Moreover, certain integrins like α9β1 are known to be essential for lymphatic valve formation and LEC differentiation, hinting that integrin-specific ECM signals could push LECs toward a lymphatic phenotype.[104] In practice, incorporating the right matrix ligand (fibronectin, collagen, laminin, *etc.*) is vital for successful lymphatic vessel engineering.

Granular hydrogels have recently been explored as scaffolds for lymphatic vasculogenesis. Montes *et al.* (2025) generated granular hydrogels (*i.e.*, jammed microgel suspensions) with tunable porosities to support 3D LEC growth (Fig. 3C). These novel granular hydrogel composites allowed LECs to form capillary-like networks and sprouts in the absence of supporting feeder cells, effectively mimicking the initial lymphatic plexus formation in a synthetic matrix. Interestingly, the microgel fabrication method (pipetting *vs.* vortexing) produced different pore size distributions that affected lymphatic sprout connectivity and maturation. Vortexed gels, which had tighter packing and smaller pores, led to earlier vessel development but slightly less interconnected networks; by contrast, pipetted gels yielded highly connected lymphatic networks, albeit with delayed sprouting.[105] Such materials-driven approaches demonstrate how matrix morphology and stiffness influence lymphatic architecture—insights that can guide tissue engineering of lymphatics and the design of pro-lymphangiogenic/vasculogenic biomaterials.

3.3 Engineering junctional phenotypes and mural cell coverage in lymphatic vessels

Understanding how LECs regulate their intercellular junctions in response to extracellular cues, and how mural cells contribute to this process, is critical for modeling both initial and collecting lymphatic functions. Henderson *et al.* (2021) pioneered an initial lymphatic vessel model, which allows direct investigation of how ECM composition influences endothelial barrier properties. In this system, human dermal LECs were seeded within a hollow microchannel encased in a 3D collagen hydrogel and cultured under luminal flow. When embedded in pure collagen I, LECs formed relatively permeable junctions, permitting the passage of macromolecules. However, when fibronectin was added to the collagen scaffold, LEC junctions tightened markedly, reducing permeability. Mechanistically, this barrier enhancement was mediated by the activation of integrin α5, either *via* fibronectin engagement or direct activation of the integrin, highlighting integrin α5 as a key regulator of lymphatic barrier integrity in response to matrix composition.[106]

Building on the theme of multicellular interaction, Selahi *et al.* (2022) introduced a more structurally faithful model of lymphatic segments—namely, the lymphangion-chip—which expands on barrier regulation by incorporating lymphatic muscle cells (LMCs) alongside LECs (Fig. 3D). Using a novel gravitational lumen patterning (GLP) technique, the researchers fabricated a microfluidic architecture comprising an endothelial channel encased by uniformly thick layers of muscle cells, closely mirroring the cylindrical structure of *in vivo* lymphangion. Under flow conditions, LECs aligned along the vessel axis while LMCs oriented circumferentially, recapitulating the native organizational pattern viewed *in vivo*. Crucially, this setup enabled real-time assessment of endothelial-mural cell communication: exposure to pro-inflammatory cytokines produced dynamic changes in LEC barrier function, mediated through LMC interactions.[107] The lymphangion-chip thus provides a versatile testbed for investigating lymphatic contractility, inflammation, and barrier dynamics in a physiologically relevant modular format.

3.4 Microfluidic control of shear stress, interstitial flow, and mechanical loading in lymphatics-on-a-chip

Careful modulation of fluid dynamics is a defining feature of lymphatics-on-a-chip systems, since LECs experience markedly lower shear stresses compared to BECs: ~0.1–2 dyne per cm^2 within initial lymphatics, *versus* 10–20 dyne per cm^2 in arterial vessels.[57] These cells are also exposed to distinct flow environments—absorbing interstitial fluid from

surrounding tissue while simultaneously transporting fluid through the lymphatic lumen. Recapitulating these different shear contexts is therefore essential for physiologically relevant lymphatic models.[98] To address this challenge, Lee *et al.* (2022) developed a multilayered microfluidic device (MμLTI-Flow) that allows simultaneous control of blood, lymphatic, and interstitial fluid pressures to model complex fluid dynamics in tissues (Fig. 3E). The system integrates engineered blood and lymphatic vessels with tunable interstitial flow, enabling direct measurement of fluid velocities and pressure-dependent transport. The authors validate the platform with computational fluid dynamics (CFD) simulations and optical microscopy, showing how luminal, transmural, and interstitial flows are interdependent rather than isolated phenomena.[112] Building on this, Ilan *et al.* (2023) developed a dual-channel lymphatic vessel-on-chip that enables precise and independent control of luminal flow, interstitial flow, both in combination, or static conditions (Fig. 3F). The device was fabricated by embedding two parallel microchannels within a 3D collagen I matrix, with one channel seeded with LECs and the adjacent acellular channel used to pressurize fluid into the surrounding hydrogel. Using this system, the authors demonstrated that interstitial flow in the presence of VEGF-C maintained discontinuous, button-like junctions and minimal sprouting, reflecting the phenotype of quiescent, highly permeable initial lymphatics. In contrast, luminal flow or combined flows in the presence of VEGF-A induced robust sprouting and more continuous, zipper-like junctions, mimicking actively remodeling collecting vessels.[108] These results highlight how LECs integrate flow cues differently depending on whether they sense fluid shear from within the lumen or across the vessel wall—an insight uniquely enabled by the two-channel design. It should be noted that VEGF isoform and flow type were varied concurrently in this design; thus, the results reflect the cooperative influence of mechanical and biochemical cues rather than an isolated causal effect of either factor. Future studies that decouple VEGF-A/-C signaling from specific flow regimens will help delineate the relative contribution of VEGFR-mediated signaling *versus* shear-dependent mechanotransduction in regulating lymphatic junction plasticity.

Complementary approaches have sought to reproduce the rhythmic dynamics of collecting lymphatics. Fathi *et al.* (2020) introduced a pumpless, gravity-driven chip in which periodic tilting of the device generated oscillatory flow through the LEC-lined channel. This design produced physiologically relevant shear stresses on the order of ~0.9 dyne per cm^2 under healthy conditions, while higher tilting rates increased shear to 6–7 dyne per cm^2, modeling pathological stress levels. Under low, physiological shear, LECs formed a stable, quiescent endothelium, whereas static conditions triggered pro-inflammatory responses, including elevated TNF-α and IL-8 secretion. Importantly, the cyclical tilting approach also simulated the intrinsic pumping activity of collecting lymphatics, generating 10 second flow pulses multiple times per minute.[113] Such platforms reveal how steady *versus* unsteady flows may elicit divergent effects on LEC biology—a subject of active investigation.

3.5 Engineering limitations and physiological gaps in current lymphatics-on-a-chip models

Although significant progress has been made in engineering lymphatic structure and function *in vitro*, several defining anatomical and physiological features of native lymphatic vessels remain difficult to reproduce. These gaps highlight the need for continued refinement of lymphatics-on-a-chip microphysiological platforms.

Lack of blind-ended initial lymphatic architecture. Most existing systems generate perfusable, continuous microvessels that resemble blood capillaries rather than the blind-ended (blunt-ended) structures characteristic of native initial lymphatics. This blind-ended morphology is not incidental; it enables pressure-driven, flap-mediated uptake of interstitial fluid and macromolecules. Its absence *in vitro* limits accurate modeling of primary lymphatic drainage, as engineered lumens tend to support convective perfusion rather than passive fluid entry across junctions.

Absence of valve-like morphogenesis in collecting lymphatics. While current platforms can recapitulate sprouting lymphangiogenesis or vasculogenesis-like network assembly, none has yet induced the morphogenetic sequence that leads to valve formation in collecting lymphatics. Mechanobiological triggers, such as oscillatory shear stress or FOXC2/PROX1 activation, can be applied *in vitro*, but downstream events including formation of valve leaflets, saddle-shaped geometries, and lymphangion organization remain unreconstituted. Without valve-like structures, *in vitro* models cannot effectively probe valve dysfunction, reflux, or transport failure.

Incomplete reconstitution of button-like junctional specialization. Although several systems demonstrate partial emergence of discontinuous VE-cadherin patterns, authentic button-like junctions remain challenging to recreate. Key *in vivo* features, including oak-leaf LEC morphology, alternating LYVE-1/VE-cadherin organization, sharply punctate junction segments, and flap-valve architecture, are only partially reproduced. These discrepancies likely reflect both incomplete mechanobiological conditioning and an incomplete understanding of the molecular programs driving button specialization. Improved insight into these pathways will be essential for engineering physiologically accurate junctions.

Together, these limitations underscore the need for next-generation lymphatic microphysiological systems capable of integrating blind-ended geometry, valve morphogenesis, and authentic junctional specialization. Continued convergence of developmental biology, mechanobiology, and microengineering will be crucial for closing these gaps. Table 2 summarizes the engineering approaches discussed in

Table 2 Engineering approaches to reconstitute lymphatic morphogenesis, junctional phenotypes, and transport functions *in vitro*

Approach	Representative features	Advantages	Limitations/challenges	Ref.
Lymphangiogenesis/sprouting	Guided LEC invasion from preformed vessels into 3D ECM (*e.g.*, collagen, fibrin) driven by interstitial flow or chemokine gradients; often mimics developmental lymphangiogenesis	• Capture early lymphangiogenic morphogenesis • Reconstitute directional growth and tip/stalk cell dynamics • Enable quantification of sprout length and branching • Allow flow conditioning	• Sprout form continuous, perfusable lumens rather than blunt-ended capillaries • Limited ability to model pressure-driven fluid entry • Require precise biochemical gradient control and matrix tuning • Typically limited to short-term culture (<1 week)	99, 101
Vasculogenesis/self-assembly	Dispersed LECs seeded within hydrogels self-organize into interconnected networks; may include stromal or perivascular support cells	• Models multicellular assembly • Support heterotypic cell interactions and spontaneous network and lumen formation • Compatible with long-term culture • Flexible for organoid co-culture	• Self-assembled networks rarely develop blind-ended termini • Authentic "oak-leaf" morphology and alternating VE-cadherin/LYVE-1 segments not reliably reproduced • Lymphangion- and valve-level organization absent • Less geometric and directional control • High heterogeneity in vessel diameter and connectivity	104, 105, 116
Flow-controlled/perfusable microchannels	LECs line predefined microchannels exposed to luminal or interstitial flow; independent control of flow direction and shear stress	• Enable direct interrogation of mechanobiology (junction remodeling, permeability, valve-like behavior) • Tunable flow environments • Support dynamic perfusion and real-time imaging	• Cannot induce morphogenesis of valve-like structures • Button-like junction markers only partially reproduced • Complex fabrication and device variability • Often lack early morphogenetic events	106, 108, 112, 113, 117
Hybrid co-culture systems	Combine lymphangiogenic sprouting with flow conditioning or stromal/immune components	• Capture multicellular crosstalk and adaptive remodeling under physiological cues • Enable modeling of lymphangiocrine signaling • Improved tissue specificity • Suitable for disease modeling	• Organ-specific lymphatic phenotypes remain incomplete • Greater experimental complexity and variability • Junctional phenotype sensitive to LEC passage number and source • Require advanced imaging and analysis workflows	100, 107, 118

this section along with their representative features, advantages, and limitations.

In summary, an expanding toolkit of microengineering strategies—ranging from 3D co-culture approaches to precisely controlled low-shear perfusion—has been integrated to construct lymphatic microphysiological systems. Each technique addresses a distinct facet of lymphatic biology, and in many cases, multiple strategies are combined within a single platform to enhance physiological relevance. Over the past decade, the field has progressed rapidly: what began as simple 2D LEC monolayers exposed to flow[88,97,119] has evolved into sophisticated 3D vessel models that closely approximate native lymphatic architecture and function for preclinical drug screening.[117,118] As the following sections will explore, these biomimetic lymphatics-on-a-chip platforms not only recapitulate fundamental aspects of lymphatic physiology but also serve as versatile tools for probing disease mechanisms and exploring therapeutics.

4 Disease applications of lymphatics-on-a-chip

Lymphatic dysfunction is implicated in a wide array of diseases, from lymphedema and inflammatory disorders to cancer metastasis and metabolic syndromes. By recreating key aspects of lymphatic physiology *in vitro*, lymphatics-on-a-chip devices have emerged as powerful tools to model these pathologies and test potential interventions. In this section, we highlight how microfluidic lymphatic models have been

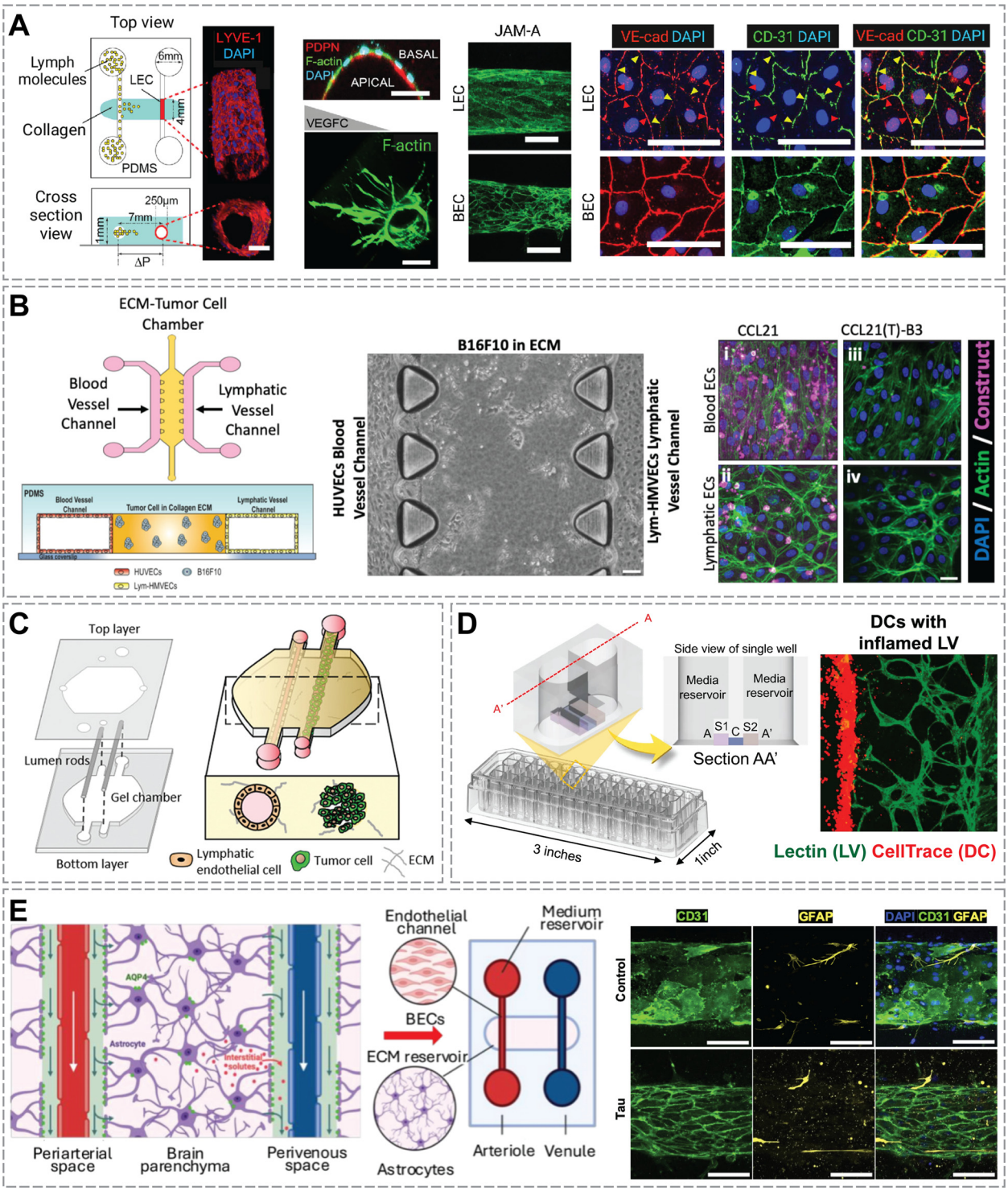

Fig. 4 Lymphatics-on-a-chip platforms for modeling lymphatic pathophysiology. (A) A schematic of the lymphatic drainage-on-chip platform. Immunostaining of lymphatic vessels and blood vessels with an adherens junction marker, VE-cadherin (VE-cad), and CD31. Red and yellow arrows indicate exclusive expression of VE-cad and CD31, respectively, showing interdigitated, discontinuous expression of VE-cad in LECs. Scale bars, 100 μm. Adapted with permission from ref. 110, copyright 2023 National Academy of Sciences. (B) TME-on-a-chip reveals that the CCL21(T)-B3 fusion construct effectively targets the tumor cells. Scale bar: 10 μm. Adapted with permission from ref. 125, copyright 2019 American Chemical Society. (C) A schematic of the breast tumor–lymphatic microfluidic device. Adapted with permission from ref. 126, copyright 2020 Wiley-VCH. (D) Illustration of an injection-molded microfluidic device designed in a 384-well plate format. Each unit contains a central channel (C) and two side channels (S1 and S2), enabling 3D LV formation and real-time tracking of DC migration. Adapted with permission from ref. 130, copyright 2025 Springer Nature. (E) Human glymphatics-on-chip model recapitulates 3D neurovascular architecture with astrocytic reactivity to tau. Scale bars: 200 μm. Adapted with permission from ref. 139, copyright 2025 American Institute of Physics.

used to simulate disease conditions, uncover disease mechanisms, and evaluate therapeutics (Fig. 4).

4.1 Modeling lymphedema pathophysiology

Lymphedema, characterized by tissue swelling due to impaired lymphatic drainage, can arise either from developmental defects (primary lymphedema) or from damage or obstruction of lymphatics (secondary lymphedema), for instance, after lymph node dissection. A hallmark feature is impaired lymph uptake and chronic inflammation in the affected tissues. Microphysiological systems have recently been leveraged to model this pathology and uncover mechanistic drivers of lymphatic dysfunction. Lee *et al.* (2023) developed a 3D lymphatic vessel-on-chip system with two parallel channels in a collagen hydrogel: one lined with LECs to mimic an initial lymphatic capillary, and the other serving as an interstitial channel for fluorescent dextran infusion (Fig. 4A). In this setup, LECs recapitulated button-like VE-cadherin junctions and supported fluid uptake akin to native initial lymphatics. However, upon exposure to inflammatory cytokines (*e.g.*, IL-2, GM-CSF, G-CSF), the chip revealed pathological junction tightening mediated by a novel ROCK2-JAM-A complex at LEC borders. This hyper-stabilization of VE-cadherin impeded fluid and protein entry, sharply reducing drainage. Importantly, ROCK inhibition restored fluid uptake, identifying ROCK2 as a potential therapeutic target for lymphedema by reversing the "blood-vessel-like" tight junction state induced by inflammation.[110] Kraus *et al.* (2023) established a human initial lymphatic primary-valve-on-a-chip in which interstitial and luminal pressures could be precisely modulated. They found that acute inflammation (*i.e.*, brief high-dose TNF-α exposure) degraded fibrillin fibers and impaired fluid uptake, but corticosteroid treatment reversed the effect. In contrast, chronic low-grade TNF-α exposure caused LEC apoptosis and persistent junctional disruption, leading to valve failure and excessive leakiness—conditions resembling advanced lymphedema.[109] This platform underscores that while acute inflammatory injury may be reversible, chronic inflammation drives irreversible valve damage, indicating the need for early anti-inflammatory intervention.

4.2 Tumor–lymphatic interactions and metastasis

The lymphatic vasculature plays a central role in metastasis, particularly as tumors exploit lymphangiogenesis to spread to regional lymph nodes. Tumors secrete growth factors such as VEGF-C and VEGF-D, which expand peritumoral lymphatics and remodel draining lymph nodes.[28] These changes facilitate tumor cell intravasation and survival in lymphatic niches.[119] Lymphatics-on-a-chip offer a unique means to study these processes under controlled conditions. The early coculture model by Pisano *et al.* (2015) showed that fluid drainage enhanced breast cancer cell invasion toward the lymphatic vessel, mediated by CCR7-CCL21 signaling, supporting the concept of autologous chemotaxis.[88] Chung *et al.* (2017) advanced this concept with a biomimetic tumor microenvironment-on-a-chip containing tumor cells, fibroblasts, and blood and lymphatic vessels. Interstitial flow and fibroblast presence promoted invasive tumor behavior and lymphatic remodeling, underscoring how stromal interactions condition lymphatic endothelium.[120] Using a one-channel microfluidic device, Gong *et al.* (2019) and Lugo-Cintrón *et al.* (2020) demonstrated that breast cancer-associated fibroblast (CAF) disrupted lymphatic vessel barrier function. Coculture with aggressive breast cancer cells exacerbated lymphatic vessel leakiness and triggered IL-6 secretion, a possible pro-metastatic mechanism of lymphatic metastasis. Blocking IL-6 signaling partially restored lymphatic barrier function, suggesting potential for vessel normalization strategies.[121,122] In a follow-up study, Lugo-Cintrón *et al.* (2021) found that tumor-derived fibroblasts dramatically increased lymphatic sprouting and network density through VEGF-C/D secretion and matrix remodeling.[123] Building on this platform, Yada *et al.* (2023) revealed that LECs secrete macrophage migration inhibitory factor (MIF), which promotes directional tumor cell migration and metabolic reprogramming toward a glycolytic phenotype. Pharmacologic inhibition of MIF reduced cancer cell motility, demonstrating that lymphatic vessels can actively drive tumor invasion through paracrine signaling rather than serving solely as passive conduits.[124]

Beyond modeling invasion, tumor–lymphatic chips are increasingly applied to therapeutic testing. Using a vascularized melanoma model, Fang *et al.* (2019) evaluated a chemokine/anti-PD-L1 nanobody fusion protein that simultaneously reshaped chemokine gradients and relieved checkpoint inhibition (Fig. 4B). This strategy enhanced T cell infiltration and anti-tumor immunity, illustrating how lymphatic chips can be harnessed to screen innovative immunotherapies.[125] Similarly, Ayuso *et al.* (2020) developed a breast cancer–lymphatic coculture platform pairing perfused LEC channels with estrogen receptor-positive (MCF-7) or triple-negative (MDA-MB-231) breast tumors (Fig. 4C). They showed that aggressive MDA-MB-231 cells reprogrammed LECs into a more inflammatory, leaky, and pro-angiogenic state than MCF-7, mirroring clinical subtype differences.[126] Frenkel *et al.* (2021) introduced immortalized human lymphatic endothelial cells (imLECs) into a membrane-free, three-lane OrganoPlate supporting continuous perfusion on a rocker platform (7° tilt, 8 min cycle) and stable biochemical gradients. The system maintained functional lymphatic microvessels for at least 18 days and enabled co-culture with colon-cancer organoids for 9 days, during which tumors induced VEGF-driven lymphatic sprouting and intravasation of cancer cells into lymphatic lumens, both effects abrogated by VEGFR-3 inhibition.[127] The platform's long-term perfusion stability and sustained lymphangiogenic activity make it a robust assay for anti-lymphangiogenic drug testing and real-time analysis of tumor intravasation.

Together, tumor–lymphatic chips now recapitulate key metastatic steps—including flow-guided invasion, stromal and matrix conditioning, subtype-specific endothelial

remodeling, and tumor intravasation—and are increasingly used to evaluate therapeutic interventions. From blocking CCR7 or IL-6 signaling to normalizing lymphatic vessels or enhancing checkpoint immunotherapy, these platforms offer powerful translational tools for dissecting and targeting the lymphatic route of cancer metastasis.

4.3 Autoimmune and inflammatory diseases

Lymphatic vessels are pivotal components of the immune system, facilitating dendritic cell (DC) and macrophage trafficking from peripheral tissues to lymph nodes, thereby priming adaptive immune responses.[128] In many chronic inflammatory conditions, such as rheumatoid arthritis and inflammatory bowel disease (IBD), lymphatic vascular remodeling is a hallmark feature. For example, in IBD, mesenteric lymphatics may undergo proliferation and contribute to the formation of tertiary lymphoid structures, which in turn hinder normal lymph flow.[2] Advances in lymphatics-on-a-chip models have propelled our understanding of immune cell migration under inflammatory conditions. Serrano *et al.* (2023) developed a microfluidic platform that recreates interstitial flow, lymphatic drainage, and immune cell recruitment on-chip. The engineered vessels achieved physiologically relevant drainage of interstitial proteins and solutes, while faithfully reproducing lymphatic-immune interactions. When peripheral blood mononuclear cells (PBMCs) were introduced under TNF-α-induced inflammatory conditions, the lymphatic chip actively recruited these immune cells; notably, blocking the chemokine receptors C–X–C motif chemokine receptor 4 (CXCR4) and CCR7 markedly reduced PBMC infiltration, demonstrating the robust modeling of chemokine-driven immune trafficking *in vitro*.[129] Complementing this, Jo *et al.* (2025) introduced a high-throughput microfluidic platform that faithfully recapitulates the structure and function of initial lymphatic vessels in a 3D environment, including DC migration governed by a CCR7-CCL21 chemokine gradient (Fig. 4D). Under conditions of elevated CCR7 expression in DCs or following TNF-α preconditioning of LECs, which induces CCL21 secretion, DCs exhibited enhanced motility and directional migration toward the lymphatic channel. However, chronic inflammation led to DC overshooting their entry, indicative of desensitization or barrier disruption.[130] These findings mirror *in vivo* observations, where acute inflammation may transiently enhance clearance, but chronic inflammation impairs trafficking efficiency.[131,132] Such systems hold promise for therapeutic screening, including TNF-α inhibition to restore DC entry dynamics and preserve LEC junctional integrity in diseases like IBD.

4.4 Neurological and glymphatic disorders

In the realm of aging and neurological disease, researchers are increasingly focusing on meningeal lymphatics[20] and the glymphatic system,[133] which together mediate cerebrospinal fluid (CSF) and interstitial solute clearance from the brain. The glymphatic pathway comprises periarterial CSF influx, astrocytic aquaporin-4 (AQP4)-mediated interstitial exchange, and perivenous efflux, functioning as a glial-dependent analogue of classical lymphatic drainage.[134] Its activity is coupled to meningeal lymphatic vessels lining the dura mater, which channel glymphatically drained CSF and solutes to the deep cervical lymph nodes.[135,136] Disruption of either pathway impairs metabolic waste clearance and has been implicated in Alzheimer's disease, traumatic brain injury, and age-related neuroinflammation.[94] Soden *et al.* (2022) developed a gliovascular unit (GVU) on-a-chip: a microfluidic platform comprised of two parallel channels embedded in a 3D hydrogel populated with human astrocytes forming AQP4-polarized endfeet with the channel lined with human brain microvascular endothelial cells. Under inflammatory stimuli (with LPS, Aβ(1–42) oligomers, or an AQP4 inhibitor), the system showed impaired clearance of fluid and Aβ(1–40) tracer introduced from the other acellular channel; drainage deficits persisted even post-cell lysis, implying roles for both cell-dependent (AQP4-related) and ECM-mediated fluid transport. Notably, inflammation depolarized AQP4, highlighting how altered localization of this channel compromises glymphatic function.[137] Building upon Soden's platform, Yslas *et al.* (2024) found that amyloid-β oligomers, but not monomers, caused pronounced astrocytic calcium signaling disruption and mislocalization of AQP4, impairing fluid clearance.[138] Park *et al.* (2025) demonstrated that hyperphosphorylated tau induced astrocytes to adopt a hypertrophic, hypercontractile phenotype, leading to vasoconstriction of the engineered vessels and reduced glymphatic clearance (Fig. 4E). Critically, pharmacological inhibition of non-muscle myosin II using blebbistatin reversed astrocytic hypercontractility, restored vessel diameter, and rescued fluid transport function.[139] By recapitulating the neural clearance pathway *in vitro*, these glymphatics-on-a-chip platforms advance our understanding of how chronic inflammation disrupts critical glymphatic functions and provide scalable systems for screening novel interventions for neurodegenerative diseases.

In summary, lymphatics-on-a-chip platforms rapidly prove their value across a broad spectrum of disease contexts. These microfluidic systems enable the dissection of complex *in vivo* phenomena—including the physical forces that impair lymph flow in lymphedema, the cellular dialogues that drive cancer dissemination through lymphatic routes, and the nuances of immune cell crosstalk and trafficking—within a controlled, tunable *in vitro* milieu. Serving both as reductionist models for mechanistic exploration and as preclinical screening platforms, these chips allow researchers to ask focused questions and test interventions with enhanced physiological relevance.

5 Future directions: toward multiscale and human-relevant lymphatic microphysiological systems

The field of lymphatics-on-a-chip is rapidly advancing but remains in an early growth phase, offering significant

potential for innovation. Several promising avenues are emerging to enhance the physiological relevance, scalability, and analytical power of these systems. In this section, we explore these future directions and discuss how they can address current limitations and open new avenues in lymphatic research and therapy (Fig. 5).

5.1 iPSC-derived lymphatic organoids and synthetic developmental programs

A major constraint in current lymphatics-on-a-chip models is the reliance on primary LECs, typically isolated from neonatal or adult skin, which may not capture the molecular and functional heterogeneity among lymphatics across different tissues (*e.g.*, gut, lung, skin, meninges, and heart). In addition to these tissue-specific constraints, commercially available human LECs also pose important demographic limitations. Neonatal or juvenile LECs are generally derived from foreskin and are therefore of male origin, whereas adult LECs are most often obtained from discarded skin collected during cosmetic procedures, which predominantly come from female donors. For researchers investigating sex-dependent or age-dependent differences in endothelial phenotypes, obtaining primary human LECs that are appropriately matched to experimental needs remains challenging. These sourcing limitations further underscore the appeal of iPSC-derived LECs as a more flexible and controllable alternative.

iPSCs offer a renewable, patient-specific source of LECs and lymphatic organoids.[140] Saha *et al.* (2024) developed a

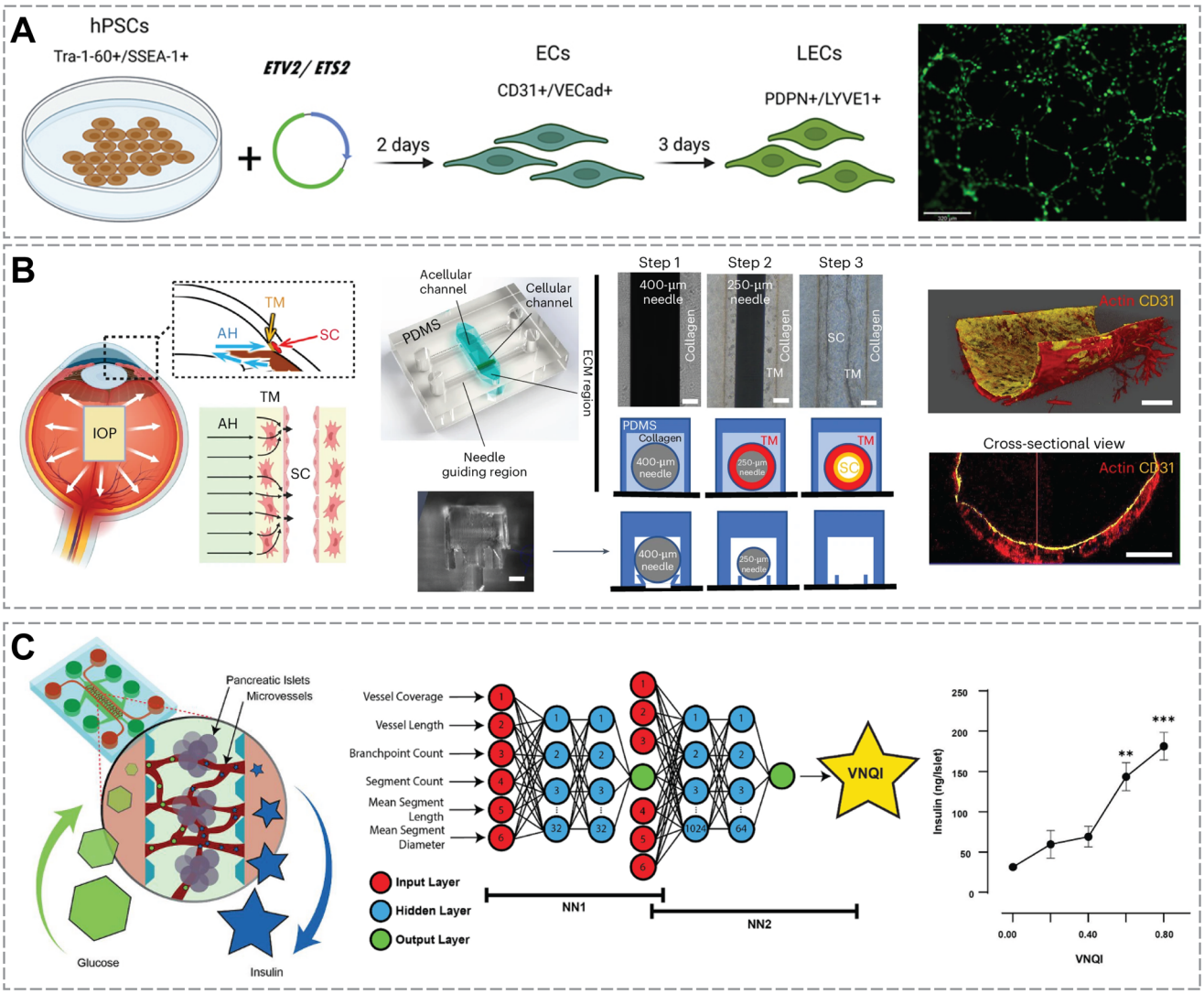

Fig. 5 Advanced engineering strategies for next-generation lymphatic microphysiological systems. (A) Schematic of deriving LECs from hiPSCs and capillary-like network formation of LEC stained by cell tracker green. Scale bar, 320 μm. Adapted with permission from ref. 34, copyright 2024 S. Karger AG. (B) The multicellular human ocular fluid outflow on-chip recapitulates steroid-induced glaucoma *in vitro*. Scale bar: 50 μm. Adapted with permission from ref. 149, copyright 2025 Springer Nature. (C) Chained neural network analysis of a cell transplant preclinical model with vascularized islet-chips designed using the VNQI. Adapted with permission from ref. 154, copyright 2023 American Institute of Chemical Engineers.

high-efficiency protocol using the transcription factors ETV2 and ETS2, with precisely timed PROX1 activation, to differentiate human iPSCs (hiPSCs) into LECs expressing VEGFR3, LYVE-1, and podoplanin at levels comparable to mature cells (Fig. 5A). These iPSC-derived LECs can assemble into stable lymphatic networks and secrete lymphangiocrine factors such as reelin, supporting their utility for *in vitro* modeling.[34] However, despite expressing key markers, iPSC-derived LECs often exhibit developmentally immature profiles, with reduced expression of valve and collector related genes (*e.g.*, FOXC2, GATA2, GJA4), incomplete junctional organization, and diminished responsiveness to mechanical cues.[34,141] These findings indicate partial functional maturity and highlight the risk of phenotypic drift over prolonged culture. Perfusion and biomechanical conditioning have shown to markedly improve the structural and metabolic maturation of iPSC-derived vascular cells.[142] Accordingly, incorporating biophysical stimuli interstitial or oscillatory flow, cyclic stretch, and matrix stiffness gradients during differentiation may help stabilize LEC identity and promote adult-like functionality.

Beyond iPSC sources, organ-specific primary LECs display distinct transcriptional and barrier properties shaped by their local microenvironments. Integrating these specialized LECs into microfluidic platforms can enhance physiological fidelity and enable comparative mechanobiological studies of regional lymphatic function. In parallel, emerging efforts to develop self-assembled vascular organoids, where ECs co-cultured with organotypic spheroids form interconnected vessel-like networks within 3D matrices, provide new avenues for modeling tissue-specific lymphatic morphogenesis.[143–145] Combining the scalability of iPSC-derived LECs with organotypic cues, co-cultures, and lymphatic organoid complexity within perfusable microfluidic systems could yield next-generation mesofluidic models that unite tissue specificity with dynamic control and real-time visualization.[146]

5.2 Organ-specific lymphatic models

Lymphatic vessels are increasingly recognized not only as conduits for fluid clearance and immune cell transport but also as active regulators of organ development, homeostasis, and tissue repair through lymphangiocrine signaling. LECs secrete a wide range of tissue-interacting factors, including metabolic cues, morphogens, chemokines, and extracellular matrix regulators, that shape the identity and function of surrounding stromal, epithelial, immune, and vascular cells.[147] Modeling these context-dependent interactions *in vitro* is therefore essential for recapitulating organ-specific lymphatic phenotypes and enhancing the physiological fidelity of organ-on-a-chip systems. By integrating lymphatic structures directly into organ-specific microphysiological platforms, researchers can interrogate how LECs influence and respond to their tissue environment. This includes immune-cell trafficking through lymphatic channels, stromal-derived guidance cues that pattern lymphatic networks, and reciprocal signaling between lymphatics and blood vessels that coordinates barrier function and antigen transport. Such systems are increasingly enabling body-on-a-chip frameworks capable of simulating drug pharmacokinetics, immune priming, and inter-organ communication.[148] A leading example is the human ocular fluid-outflow chip developed by Lu *et al.* (2025), which reconstructs the trabecular meshwork (TM) and the lymphatic-like Schlemm's canal (SC) using a dual-layer microfluidic architecture (Fig. 5B).[149] This platform recapitulates human aqueous humor drainage by channeling interstitial flow through an SC endothelial compartment enveloped by TM. Under steroid exposure, the chip reproduces hallmark features of steroid-induced glaucoma, including impaired fluid egress and strengthened SC junctions, mediated by an ALK5-VEGFC signaling axis between TM and SC cells. This work illustrates how emergent disease phenotypes require heterotypic interactions, which are not captured in monoculture systems, and positions the platform for incorporation into multi-organ models.

Beyond the ocular niche, lymph node-on-a-chip technologies have emerged as powerful models for studying lymphatic-immune communication within a structured lymphoid microenvironment.[150–152] These platforms recreate subcapsular sinus flow, fibroblastic reticular cell networks, and LEC-immune cell interactions, enabling precise examination of antigen capture, dendritic cell transit, and flow-dependent lymphocyte activation. Multi-compartment organ-on-chip frameworks can further couple peripheral tissue modules to downstream lymph node chambers *via* perfused lymphatic channels, thereby recreating antigen drainage, cytokine transport, and immune priming in a human-relevant context. Such integration will be crucial for mechanistic studies of how local lymphatic function shapes systemic immunity and immunotherapy responses.

Several additional organ systems present compelling opportunities for lymphatic modeling. Intestinal lacteals coordinate with enterocytes and immune cells to mediate chylomicron uptake and are susceptible to VEGF-A-driven junction zippering in obesity.[2,14,38] Adipose lymphatics regulate lipid mobilization and inflammatory tone; their dysfunction, as seen with CD36 loss, promotes visceral inflammation and insulin resistance mirroring type 2 diabetes.[12] Microfluidic co-cultures incorporating LECs with adipocytes, enterocytes, renal epithelial cells, or meningeal stromal cells could recapitulate these organ-specific pathophysiologies. Renal and meningeal lymphatic-epithelial chips may further model fibrotic fluid imbalance, intracranial pressure dynamics, and CSF clearance defects relevant to neurodegenerative disease.

Together, these emerging organ-specific and immune-linked lymphatics-on-a-chip platforms illustrate the importance of heterotypic, lymphangiocrine interactions in shaping lymphatic structure and function across tissues. Coupling patient-derived cells, autologous immune

components, or disease-relevant organoids with perfusable lymphatic channels will enable personalized mechanistic studies and therapeutic testing across diverse organ systems—from lymph nodes and the eye to intestine, adipose tissue, kidney, brain, and beyond.

5.3 Computational and AI-assisted design of lymphatic networks

As lymphatics-on-a-chip systems grow increasingly sophisticated, they generate rich, high-dimensional datasets that are challenging to interpret using conventional analysis. This complexity presents a compelling opportunity for AI to bridge empirical experimentation and mechanistic understanding. AI offers powerful tools for handling multivariate perturbation experiments typical of lymphatic microfluidic studies. For instance, microfluidics methods have already used evolutionary algorithms to engineer channel geometries optimized for uniform shear stress or physiologically realistic flow distribution.[153–155] Such methods could be adapted to lymphatic chips to tailor microchannel networks that mimic native interstitial flow or lymph propulsion dynamics. A landmark advance in applying AI to vascular—and by extension lymphatic—networks comes from the work of Tronolone *et al.* (2023), who developed a Vascular Network Quality Index (VNQI) using supervised machine learning and a chained neural network architecture (Fig. 5C). This index compresses complex vascular morphology into a single predictive metric that correlates strongly with functional oxygen transport—outperforming simpler morphological measures alone.[154] Applied to lymphatics, a similar index could quantify network efficiency in terms of fluid clearance, immune cell trafficking, or barrier integrity, based on features like valve density, contractile behavior, and junctional permeability.

Looking ahead, AI-enabled systems could evolve toward adaptive experimental frameworks, where AI "agents" monitor real-time readouts (*e.g.*, flow dynamics, cell migration) and actively modulate stimuli (*e.g.*, growth factors, mechanical stress) to optimize outcomes. Such closed-loop experimentation would dramatically accelerate optimization of drug delivery conditions or personalized therapeutic regimens on a chip. Currently, lymphatics-on-a-chip studies are often proof-of-concept or limited in throughput. Integrating AI and machine learning, coupled with high-throughput microfluidic platforms,[156] 3D bioprinting,[157,158] and advanced microfabrication,[159] promises to scale these systems—transforming them from single-use demonstrations into robust screening tools that accelerate drug discovery and mechanistic exploration.

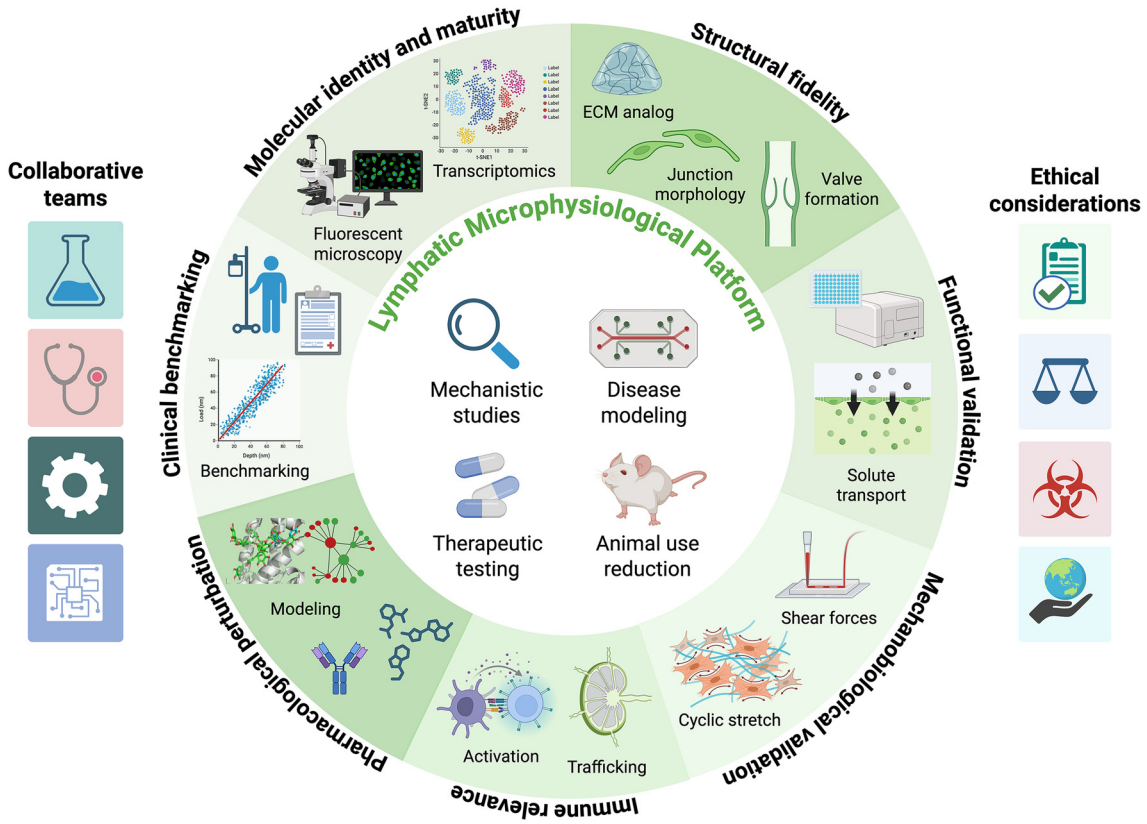

Fig. 6 Multilevel validation framework for human lymphatic microphysiological systems. Schematic illustrating a multilevel validation framework for human lymphatics-on-a-chip systems, encompassing molecular, structural, functional, and clinical benchmarks. Adapted with permission from ref. 160, copyright 2024 Elsevier. Created with https://BioRender.com.

5.4 Standards for validation of human lymphatic microphysiological platforms

Establishing robust validation criteria is essential to ensure that human lymphatics-on-a-chip accurately recapitulate native vessel identity, structure, and function (Fig. 6). Validation should begin with confirming molecular identity and maturity, including expression of canonical lymphatic markers (PROX1, VEGFR-3, PDPN, LYVE-1) and junctional proteins (VE-cadherin, CLDN5), together with valve-associated regulators such as FOXC2 and GATA2 that signify developmental progression. Structural fidelity can be assessed through imaging of button- *versus* zipper-like junctions, oak-leaf LEC overlaps, and anchoring-filament analogs that maintain tissue attachment. Functional validation should demonstrate physiologically relevant solute and macromolecule transport, quantified by tracer uptake and size-selective permeability assays.

Mechanobiological validation involves confirming flow-dependent behaviors, such as junctional remodeling, nitric-oxide signaling, and cyclic-stretch responses, that mimic pumping and valve dynamics in collecting vessels. Immune relevance can be established by assessing CCR7-dependent DC and T cell transmigration toward CCL21 gradients, and by testing cytokine-induced barrier modulation under TNF-α or IL-1β stimulation. Pharmacological perturbations provide further functional benchmarks, including expected changes in contractility or permeability following VEGF-A/C or VEGFR-3 blockade, RhoA/ROCK inhibition, or glucocorticoid treatment.

Finally, quantitative benchmarking against human data, encompassing histological architecture, lymphangiography or intralymphatic imaging, and tracer-clearance kinetics, should be reported with clear effect sizes and scaling assumptions to facilitate reproducibility and cross-platform comparison. Collectively, these integrated strategies provide a rigorous foundation for validating human lymphatic microphysiological systems and advancing them as reproducible, predictive tools for both disease modeling and therapeutic testing.

6 Conclusion

In closing, the future of lymphatics-on-a-chip is auspicious, poised to accelerate therapeutic innovation across domains—from lymphedema interventions and immunotherapies to vaccines leveraging lymphatic transport to lymph nodes. These microphysiological systems offer unprecedented potential to accurately replicate human lymphatic physiology and disease, complementing and even replacing traditional animal models, which suffer from translational limitations and rising regulatory and ethical scrutiny. As integrated platforms—combining lymphatic, immune, and multi-organ functionality—continue to materialize, they align tightly with advances in personalized medicine, high-throughput screening, and translational science, drawing on multidisciplinary collaboration across engineering, biology, and computation. For a system as historically underappreciated and complex as the lymphatic vasculature, these advances come at a pivotal time, ensuring that the next generations of lymphatics-on-a-chip models are ever more physiological, predictive, and useful in unraveling the mysteries of the lymphatic system.

Author contributions

Writing – original draft: Y. P. Writing – review & editing: Y. P., E. L.

Conflicts of interest

There are no conflicts to declare.

Data availability

No primary research results, software or code have been included and no new data were generated or analysed as part of this review.

Acknowledgements

This work was supported by NIH grants (CA279560, HL165135). Y. P. was supported by the International Foundation for Ethical Research (IFER) Fellowship.

References

1 L. Alderfer, A. Wei and D. Hanjaya-Putra, *J. Biol. Eng.*, 2018, **12**, 32.
2 B. J. Mehrara, A. J. Radtke, G. J. Randolph, B. T. Wachter, P. Greenwel, I. I. Rovira, Z. S. Galis and S. C. Muratoglu, *J. Clin. Invest.*, 2023, **133**, e171582.
3 G. Oliver, J. Kipnis, G. J. Randolph and N. L. Harvey, *Cell*, 2020, **182**, 270–296.
4 T. Karakousi, T. Mudianto and A. W. Lund, *Nat. Rev. Cancer*, 2024, **24**, 363–381.
5 N. Schwartz, M. L. S. Chalasani, T. M. Li, Z. Feng, W. D. Shipman and T. T. Lu, *Front. Immunol.*, 2019, **10**, 519.
6 R. Hokari and A. Tomioka, *Inflammation Regener.*, 2021, **41**, 25.
7 L. Zhang, D. K. W. Ocansey, L. Liu, C. V. Olovo, X. Zhang, H. Qian, W. Xu and F. Mao, *Biomed. Pharmacother.*, 2021, **140**, 111752.
8 D. Nikolakis, F. A. E. De Voogd, M. J. Pruijt, J. Grootjans, M. G. Van De Sande and G. R. D'Haens, *IJMS*, 2022, **23**, 1854.
9 B. N. K. Ruliffson and C. F. Whittington, *Adv. Biol.*, 2023, e2200158, DOI: 10.1002/adbi.202200158.
10 N. Escobedo and G. Oliver, *Cell Metab.*, 2017, **26**, 598–609.
11 R. P. Kataru, H. J. Park, J. E. Baik, C. Li, J. Shin and B. J. Mehrara, *Front. Physiol.*, 2020, **11**, 459.
12 V. Cifarelli, S. Appak-Baskoy, V. S. Peche, A. Kluzak, T. Shew, R. Narendran, K. M. Pietka, M. Cella, C. W. Walls, R. Czepielewski, S. Ivanov, G. J. Randolph, H. G. Augustin and N. A. Abumrad, *Nat. Commun.*, 2021, **12**, 3350.
13 E. Cao, M. J. Watt, C. J. Nowell, T. Quach, J. S. Simpson, V. De Melo Ferreira, S. Agarwal, H. Chu, A. Srivastava, D.

Anderson, G. Gracia, A. Lam, G. Segal, J. Hong, L. Hu, K. L. Phang, A. B. J. Escott, J. A. Windsor, A. R. J. Phillips, D. J. Creek, N. L. Harvey, C. J. H. Porter and N. L. Trevaskis, *Nat. Metab.*, 2021, **3**, 1175–1188.

14 G. Zarkada, X. Chen, X. Zhou, M. Lange, L. Zeng, W. Lv, X. Zhang, Y. Li, W. Zhou, K. Liu, D. Chen, N. Ricard, J. Liao, Y.-B. Kim, R. Benedito, L. Claesson-Welsh, K. Alitalo, M. Simons, R. Ju, X. Li, A. Eichmann and F. Zhang, *Circ. Res.*, 2023, **133**, 333–349.

15 E. Brakenhielm and K. Alitalo, *Nat. Rev. Cardiol.*, 2019, **16**, 56–68.

16 K. Klaourakis, J. M. Vieira and P. R. Riley, *Nat. Rev. Cardiol.*, 2021, **18**, 368–379.

17 X. Liu and G. Oliver, *Circ. Res.*, 2023, **132**, 1246–1253.

18 A. Louveau, S. Da Mesquita and J. Kipnis, *Neuron*, 2016, **91**, 957–973.

19 B.-L. Sun, L.-h. Wang, T. Yang, J.-y. Sun, L.-l. Mao, M.-f. Yang, H. Yuan, R. A. Colvin and X.-y. Yang, *Prog. Neurobiol.*, 2018, **163–164**, 118–143.

20 Q. Zhang, Y. Niu, Y. Li, C. Xia, Z. Chen, Y. Chen and H. Feng, *Signal Transduction Targeted Ther.*, 2025, **10**, 142.

21 L. Gutierrez-Miranda and K. Yaniv, *Front. Physiol.*, 2020, **11**, 577584.

22 M. Sun, J. Angelillo and S. Hugues, *J. Exp. Med.*, 2025, **222**, e20231954.

23 W. J. Polacheck, J. B. Dixon and W. Y. Aw, *Annu. Rev. Biomed. Eng.*, 2025, **27**, 73–100.

24 C. Ma, Y. Peng, H. Li and W. Chen, *Trends Pharmacol. Sci.*, 2020, **42**, 119–133.

25 M. Skobe, T. Hawighorst, D. G. Jackson, R. Prevo, L. Janes, P. Velasco, L. Riccardi, K. Alitalo, K. Claffey and M. Detmar, *Nat. Med.*, 2001, **7**, 192–198.

26 T. Karpanen, M. Egeblad, M. J. Karkkainen, H. Kubo, S. Ylä-Herttuala, M. Jäättelä and K. Alitalo, *Cancer Res.*, 2001, **61**, 1786–1790.

27 J. Krishnan, V. Kirkin, A. Steffen, M. Hegen, D. Weih, S. Tomarev, J. r. Wilting and J. P. Sleeman, *Cancer Res.*, 2003, **63**, 713–722.

28 K. Alitalo, T. Tammela and T. V. Petrova, *Nature*, 2005, **438**, 946–953.

29 S. Zhang, S. Yi, D. Zhang, M. Gong, Y. Cai and L. Zou, *Sci. Rep.*, 2017, **7**, 40364.

30 J. Li, Y.-B. Liang, Q.-B. Wang, Y.-K. Li, X.-M. Chen, W.-L. Luo, Y. Lakang, Z.-S. Yang, Y. Wang, Z.-W. Li and Y. Ke, *Front. Immunol.*, 2025, **15**, 1519999.

31 I. Van Der Auwera, Y. Cao, J. C. Tille, M. S. Pepper, D. G. Jackson, S. B. Fox, A. L. Harris, L. Y. Dirix and P. B. Vermeulen, *Br. J. Cancer*, 2006, **95**, 1611–1625.

32 N. Audet, N. J. Beasley, C. Macmillan, D. G. Jackson, P. J. Gullane and S. Kamel-Reid, *Arch. Otolaryngol., Head Neck Surg.*, 2005, **131**, 1065.

33 I.-E. Lupu, D. E. Grainger, N. Kirschnick, S. Weischer, E. Zhao, I. Martinez-Corral, H. Schoofs, M. Vanhollebeke, G. Jones, J. Godwin, A. Forrow, I. Lahmann, P. R. Riley, T. Zobel, K. Alitalo, T. Mäkinen, F. Kiefer and O. A. Stone, *Nat. Cardiovasc. Res.*, 2025, **4**, 45–63.

34 S. Saha, F. Graham, J. Knopp, C. Patzke and D. Hanjaya-Putra, *Cells Tissues Organs*, 2024, 1–11, DOI: 10.1159/000539699.

35 M. Jannaway, D. Iyer, D. M. Mastrogiacomo, K. Li, D. C. Sung, Y. Yang, M. L. Kahn and J. P. Scallan, *Cell Rep.*, 2023, **42**, 112777.

36 H. Schoofs and T. Mäkinen, *Int. J. Dev. Biol.*, 2024, **68**, 189–198.

37 I. Martinez-Corral, M. H. Ulvmar, L. Stanczuk, F. Tatin, K. Kizhatil, S. W. M. John, K. Alitalo, S. Ortega and T. Makinen, *Circ. Res.*, 2015, **116**, 1649–1654.

38 F. Zhang, G. Zarkada, J. Han, J. Li, A. Dubrac, R. Ola, G. Genet, K. Boyé, P. Michon, S. E. Künzel, J. P. Camporez, A. K. Singh, G.-H. Fong, M. Simons, P. Tso, C. Fernández-Hernando, G. I. Shulman, W. C. Sessa and A. Eichmann, *Science*, 2018, **361**, 599–603.

39 V. Cifarelli and A. Eichmann, *Cell. Mol. Gastroenterol. Hepatol.*, 2019, **7**, 503–513.

40 T. V. Petrova and G. Y. Koh, *Science*, 2020, **369**, eaax4063.

41 A. F. M. Salvador, N. Abduljawad and J. Kipnis, *Annu. Rev. Neurosci.*, 2024, **47**, 323–344.

42 P. R. Norden and T. Kume, *Front. Cell Dev. Biol.*, 2020, **8**, 627647.

43 F. Zhang, G. Zarkada, S. Yi and A. Eichmann, *Front. Physiol.*, 2020, **11**, 509.

44 J. E. Moore, Jr. and C. D. Bertram, *Annu. Rev. Fluid Mech.*, 2018, **50**, 459–482.

45 M. A. Swartz and A. W. Lund, *Nat. Rev. Cancer*, 2012, **12**, 210–219.

46 J. Amersfoort, G. Eelen and P. Carmeliet, *Nat. Rev. Immunol.*, 2022, **22**, 576–588.

47 H. Schoofs, N. Daubel, S. Schnabellehner, M. L. B. Gronloh, S. Palacios Martinez, A. Halme, A. M. Marks, M. Jeansson, S. Barcos, C. Brakebusch, R. Benedito, B. Engelhardt, D. Vestweber, K. Gaengel, F. Linsenmeier, S. Schurmann, P. Saharinen, J. D. van Buul, O. Friedrich, R. S. Smith, M. Majda and T. Makinen, *Nature*, 2025, **641**, 465–475.

48 S. Fu, Y. Wang, E. Bin, H. Huang, F. Wang and N. Tang, *Proc. Natl. Acad. Sci. U. S. A.*, 2023, **120**, e2215449120.

49 M. Frye, S. Stritt, H. Ortsäter, M. Hernandez Vasquez, M. Kaakinen, A. Vicente, J. Wiseman, L. Eklund, J. L. Martínez-Torrecuadrada, D. Vestweber and T. Mäkinen, *eLife*, 2020, **9**, e57732.

50 W. E. Cromer, S. D. Zawieja, B. Tharakan, E. W. Childs, M. K. Newell and D. C. Zawieja, *Angiogenesis*, 2014, **17**, 395–406.

51 P. Baluk, J. Fuxe, H. Hashizume, T. Romano, E. Lashnits, S. Butz, D. Vestweber, M. Corada, C. Molendini, E. Dejana and D. M. McDonald, *J. Exp. Med*, 2007, **204**, 2349–2362.

52 L.-C. Yao, P. Baluk, R. S. Srinivasan, G. Oliver and D. M. Mcdonald, *Am. J. Pathol.*, 2012, **180**, 2561–2575.

53 M. J. Davis, S. D. Zawieja and Y. Yang, *Front. Cell Dev. Biol.*, 2024, **12**, 1331291.

54 D. Iyer, D. M. Mastrogiacomo, K. Li, R. Banerjee, Y. Yang and J. P. Scallan, *Arterioscler., Thromb., Vasc. Biol.*, 2023, **43**, 2197–2212.

55 T. V. Petrova, T. Karpanen, C. Norrmén, R. Mellor, T. Tamakoshi, D. Finegold, R. Ferrell, D. Kerjaschki, P. Mortimer, S. Ylä-Herttuala, N. Miura and K. Alitalo, *Nat. Med.*, 2004, **10**, 974–981.
56 A. Sabine, Y. Agalarov, H. M.-E. Hajjami, M. Jaquet, R. Hägerling, C. Pollmann, D. Bebber, A. Pfenniger, N. Miura, O. Dormond, J.-M. Calmes, R. H. Adams, T. Mäkinen, F. Kiefer, B. R. Kwak and T. V. Petrova, *Dev. Cell*, 2012, **22**, 430–445.
57 D. Choi, E. Park, E. Jung, Y. J. Seong, J. Yoo, E. Lee, M. Hong, S. Lee, H. Ishida, J. Burford, J. Peti-Peterdi, R. H. Adams, S. Srikanth, Y. Gwack, C. S. Chen, H. J. Vogel, C. J. Koh, A. K. Wong and Y.-K. Hong, *J. Clin. Invest.*, 2017, **127**, 1225–1240.
58 M. N. Hernández Vásquez, M. H. Ulvmar, A. González-Loyola, I. Kritikos, Y. Sun, L. He, C. Halin, T. V. Petrova and T. Mäkinen, *EMBO J.*, 2021, **40**, EMBJ2020107192.
59 K. Nonomura, V. Lukacs, D. T. Sweet, L. M. Goddard, A. Kanie, T. Whitwam, S. S. Ranade, T. Fujimori, M. L. Kahn and A. Patapoutian, *Proc. Natl. Acad. Sci. U. S. A.*, 2018, **115**, 12817–12822.
60 D. Choi, E. Park, J. Choi, R. Lu, J. S. Yu, C. Kim, L. Zhao, J. Yu, B. Nakashima, S. Lee, D. Singhal, J. P. Scallan, B. Zhou, C. J. Koh, E. Lee and Y.-K. Hong, *Nat. Neurosci.*, 2024, **27**, 913–926.
61 L. Planas-Paz, B. Strilić, A. Goedecke, G. Breier, R. Fässler and E. Lammert, *EMBO J.*, 2012, **31**, 788–804.
62 N. Baeyens, S. Nicoli, B. G. Coon, T. D. Ross, K. Van den Dries, J. Han, H. M. Lauridsen, C. O. Mejean, A. Eichmann, J.-L. Thomas, J. D. Humphrey and M. A. Schwartz, *eLife*, 2015, **4**, e04645.
63 V. Angeli and H. Y. Lim, *Cell. Mol. Immunol.*, 2023, **20**, 1051–1062.
64 C. Bonvin, J. Overney, A. C. Shieh, J. B. Dixon and M. A. Swartz, *Biotechnol. Bioeng.*, 2010, **105**, 982–991.
65 D. Choi, E. Park, E. Jung, Y. J. Seong, M. Hong, S. Lee, J. Burford, G. Gyarmati, J. Peti-Peterdi, S. Srikanth, Y. Gwack, C. J. Koh, E. Boriushkin, A. Hamik, A. K. Wong and Y.-K. Hong, *Circ. Res.*, 2017, **120**, 1426–1439.
66 H. Wiig and H. Noddeland, *Scand. J. Clin. Lab. Invest.*, 1983, **43**, 255–260.
67 E. Stranden and H. O. Myhre, *Microvasc. Res.*, 1982, **24**, 241–248.
68 S. Jamalian, M. Jafarnejad, S. D. Zawieja, C. D. Bertram, A. A. Gashev, D. C. Zawieja, M. J. Davis and J. E. Moore, *Sci. Rep.*, 2017, **7**, 12080.
69 Y. L. Huang, J. E. Segall and M. Wu, *Lab Chip*, 2017, **17**, 3221–3233.
70 S. R. Chary and R. K. Jain, *Proc. Natl. Acad. Sci. U. S. A.*, 1989, **86**, 5385–5389.
71 D. Negrini and M. Del Fabbro, *J. Physiol.*, 1999, **520**, 761–769.
72 D. Negrini, A. Moriondo and S. Mukenge, *Lymphatic Res. Biol.*, 2004, **2**, 69–81.
73 A. Moriondo, S. Mukenge and D. Negrini, *Am. J. Physiol.*, 2005, **289**, H263–H269.
74 G. Clough and L. H. Smaje, *J. Physiol.*, 1978, **283**, 457–468.
75 E. M. Bouta, R. W. Wood, E. B. Brown, H. Rahimi, C. T. Ritchlin and E. M. Schwarz, *J. Physiol.*, 2014, **592**, 1213–1223.
76 J. P. Scallan and V. H. Huxley, *J. Physiol.*, 2010, **588**, 243–254.
77 H. J. T. Guthe, M. Indrebø, T. Nedrebø, G. Norgård, H. Wiig and A. Berg, *PLoS One*, 2015, **10**, e0122779.
78 J. K. Heltne, P. Husby, M. E. Koller and T. Lund, *Lab. Anim.*, 1998, **32**, 439–445.
79 R. D. Manning, *Am. J. Physiol.*, 1998, **275**, R135–R140.
80 K. Aukland, G. C. Kramer and E. M. Renkin, *Am. J. Physiol.*, 1984, **247**, H74–H79.
81 D. A. Berk, M. A. Swartz, A. J. Leu and R. K. Jain, *Am. J. Physiol.*, 1996, **270**, H330–H337.
82 M. Fischer, U. K. Franzeck, I. Herrig, U. Costanzo, S. Wen, M. Schiesser, U. Hoffmann and A. Bollinger, *Am. J. Physiol.*, 1996, **270**, H358–H363.
83 J. B. Dixon, S. T. Greiner, A. A. Gashev, G. L. Cote, J. E. Moore and D. C. Zawieja, *Microcirculation*, 2006, **13**, 597–610.
84 C. Blatter, E. F. J. Meijer, A. S. Nam, D. Jones, B. E. Bouma, T. P. Padera and B. J. Vakoc, *Sci. Rep.*, 2016, **6**, 29035.
85 E. Rahbar, T. Akl, G. L. Coté, J. E. Moore and D. C. Zawieja, *Microcirculation*, 2014, **21**, 359–367.
86 S. Molloi, A. R. Polivka, Y. Zhao, J. Redmond, M. Itkin, I. Antunes and Z. Yu, *Radiology*, 2023, **309**, e230959.
87 M. Jafarnejad, W. E. Cromer, R. R. Kaunas, S. L. Zhang, D. C. Zawieja and J. E. Moore, Jr., *Am. J. Physiol.*, 2015, **308**, H697–H706.
88 M. Pisano, V. Triacca, K. A. Barbee and M. A. Swartz, *Integr. Biol.*, 2015, **7**, 525–533.
89 A. A. Gashev, M. J. Davis, M. D. Delp and D. C. Zawieja, *Microcirculation*, 2004, **11**, 477–492.
90 H. Cheon, S. H. Lee, S. A. Kim, B. Kim, H. P. Suh and J. Y. Jeon, *Arterioscler., Thromb., Vasc. Biol.*, 2023, **43**, 2008–2022.
91 J.-P. Belgrado, L. Vandermeeren, S. Vankerckhove, J.-B. Valsamis, J. Malloizel-Delaunay, J.-J. Moraine and F. Liebens, *Lymphatic Res. Biol.*, 2016, **14**, 70–77.
92 J. W. Breslin, *Microvasc. Res.*, 2014, **96**, 46–54.
93 J. P. Scallan, S. D. Zawieja, J. A. Castorena-Gonzalez and M. J. Davis, *J. Physiol.*, 2016, **594**, 5749–5768.
94 J. Hagendoorn, T. P. Padera, S. Kashiwagi, N. Isaka, F. Noda, M. I. Lin, P. L. Huang, W. C. Sessa, D. Fukumura and R. K. Jain, *Circ. Res.*, 2004, **95**, 204–209.
95 M. Jannaway and J. P. Scallan, *Front. Physiol.*, 2021, **12**, 687563.
96 K. H. K. Wong, J. G. Truslow, A. H. Khankhel, K. L. S. Chan and J. Tien, *J. Biomed. Mater. Res., Part A*, 2013, **101**, 2181–2190.
97 M. Sato, N. Sasaki, M. Ato, S. Hirakawa, K. Sato and K. Sato, *PLoS One*, 2015, **10**, e0137301.
98 E. Hall, K. Mendiola, N. K. Lightsey and D. Hanjaya-Putra, *Biomicrofluidics*, 2024, **18**, 031502.
99 S. Kim, M. Chung and N. L. Jeon, *Biomaterials*, 2016, **78**, 115–128.

100 T. Osaki, J. C. Serrano and R. D. Kamm, *Regener. Eng. Transl. Med.*, 2018, **4**, 120–132.
101 J. J. Tronolone, N. Mohamed and A. Jain, *Adv. Biol.*, 2024, **8**, e2400031.
102 L. Gibot, T. Galbraith, J. Bourland, A. Rogic, M. Skobe and F. A. Auger, *Nat. Protoc.*, 2017, **12**, 1077–1088.
103 F. Fan, B. Su, A. Kolodychak, E. Ekwueme, L. Alderfer, S. Saha, M. J. Webber and D. Hanjaya-Putra, *ACS Appl. Mater. Interfaces*, 2023, **15**, 58181–58195.
104 L. Alderfer, S. Saha, F. Fan, J. Wu, L. E. Littlepage and D. Hanjaya-Putra, *Commun. Biol.*, 2024, **7**, 1262.
105 D. Montes, S. Saha, A. Taglione, D. P. Jeong, L. Chen, F. Fan, H. C. Chang and D. Hanjaya-Putra, *Adv. Mater. Interfaces*, 2025, **12**, 2401037.
106 A. R. Henderson, I. S. Ilan and E. Lee, *Microcirculation*, 2021, **28**, e12730.
107 A. Selahi, T. Fernando, S. Chakraborty, M. Muthuchamy, D. C. Zawieja and A. Jain, *Lab Chip*, 2022, **22**, 121–135.
108 I. S. Ilan, A. R. Yslas, Y. Peng, R. Lu and E. Lee, *Cell. Mol. Bioeng.*, 2023, **16**, 325–339.
109 S. Kraus and E. Lee, *Lab Chip*, 2023, **23**, 5180–5194.
110 E. Lee, S.-L. Chan, Y. Lee, W. J. Polacheck, S. Kwak, A. Wen, D.-H. T. Nguyen, M. L. Kutys, S. Alimperti, A. M. Kolarzyk, T. J. Kwak, J. Eyckmans, D. R. Bielenberg, H. Chen and C. S. Chen, *Proc. Natl. Acad. Sci. U. S. A.*, 2023, **120**, e2308941120.
111 A. Selahi, S. Chakraborty, M. Muthuchamy, D. C. Zawieja and A. Jain, *Analyst*, 2022, **147**, 2953–2965.
112 G. H. Lee, S. A. Huang, W. Y. Aw, M. L. Rathod, C. Cho, F. S. Ligler and W. J. Polacheck, *Biofabrication*, 2022, **14**, 025007.
113 P. Fathi, G. Holland, D. Pan and M. B. Esch, *ACS Appl. Bio Mater.*, 2020, **3**, 6697–6707.
114 M. Frye, A. Taddei, C. Dierkes, I. Martinez-Corral, M. Fielden, H. Ortsäter, J. Kazenwadel, D. P. Calado, P. Ostergaard, M. Salminen, L. He, N. L. Harvey, F. Kiefer and T. Mäkinen, *Nat. Commun.*, 2018, **9**, 1511.
115 E. Gordon, L. Schimmel and M. Frye, *Front. Physiol.*, 2020, **11**, 684.
116 L. Alderfer, E. Russo, A. Archilla, B. Coe and D. Hanjaya-Putra, *FASEB J.*, 2021, **35**, e21498.
117 R. Lu, B. J. Lee and E. Lee, *ACS Biomater. Sci. Eng.*, 2024, **10**, 5752–5763.
118 A. M. Ledo, G. Misiewicz, T. Dimke, W. R. Tschantz, J. Handel, R. Pelis, G. Bruin, K. Bechtold-Peters, M. Sanchez-Felix, S. Deshmukh, S. Kim, M. Proestaki and R. D. Kamm, *Lab Chip*, 2025, **25**, 4660–4676.
119 J. D. Shields, M. E. Fleury, C. Yong, A. A. Tomei, G. J. Randolph and M. A. Swartz, *Cancer Cell*, 2007, **11**, 526–538.
120 M. Chung, J. Ahn, K. Son, S. Kim and N. L. Jeon, *Adv. Healthcare Mater.*, 2017, **6**, 1700196.
121 M. M. Gong, K. M. Lugo-Cintron, B. R. White, S. C. Kerr, P. M. Harari and D. J. Beebe, *Biomaterials*, 2019, **214**, 119225.
122 K. M. Lugo-Cintrón, J. M. Ayuso, B. R. White, P. M. Harari, S. M. Ponik, D. J. Beebe, M. M. Gong and M. Virumbrales-Muñoz, *Lab Chip*, 2020, **20**, 1586–1600.
123 K. M. Lugo-Cintrón, J. M. Ayuso, M. Humayun, M. M. Gong, S. C. Kerr, S. M. Ponik, P. M. Harari, M. Virumbrales-Muñoz and D. J. Beebe, *EBioMedicine*, 2021, **73**, 103634.
124 R. C. Yada, D. E. Desa, A. A. Gillette, E. Bartels, P. M. Harari, M. C. Skala, D. J. Beebe and S. C. Kerr, *Biomaterials*, 2023, **298**, 122136.
125 T. Fang, R. Li, Z. Li, J. Cho, J. S. Guzman, R. D. Kamm and H. L. Ploegh, *Mol. Pharmaceutics*, 2019, **16**, 2838–2844.
126 J. M. Ayuso, M. M. Gong, M. C. Skala, P. M. Harari and D. J. Beebe, *Adv. Healthcare Mater.*, 2020, **9**, 1900925.
127 N. Frenkel, S. Poghosyan, C. R. Alarcon, S. B. Garcia, K. Queiroz, L. van den Bent, J. Laoukili, I. B. Rinkes, P. Vulto, O. Kranenburg and J. Hagendoorn, *ACS Biomater. Sci. Eng.*, 2021, **7**, 3030–3042.
128 C. Viúdez-Pareja, E. Kreft and M. García-Caballero, *Front. Immunol.*, 2023, **14**, 1235812.
129 J. C. Serrano, M. R. Gillrie, R. Li, S. H. Ishamuddin, E. Moeendarbary and R. D. Kamm, *Adv. Sci.*, 2023, **11**, 2302903.
130 H. Jo, S. Lee, I. Park, M. Shim, J. Yu, Y. S. Oh, J. Doh, Y.-K. Hong and N. L. Jeon, *BioChip J.*, 2025, **19**, 227.
131 V. Angeli and G. J. Randolph, *Lymphatic Res. Biol.*, 2006, **4**, 217–228.
132 A. J. Christiansen, L. C. Dieterich, I. Ohs, S. B. Bachmann, R. Bianchi, S. T. Proulx, M. Hollmén, D. Aebischer and M. Detmar, *Oncotarget*, 2016, **7**, 39421–39435.
133 K. Ayyappan, L. Unger, P. Kitchen, R. M. Bill and M. M. Salman, *Neural Regener. Res.*, 2026, **21**, 534–541.
134 J. J. Iliff, M. Wang, Y. Liao, B. A. Plogg, W. Peng, G. A. Gundersen, H. Benveniste, G. E. Vates, R. Deane, S. A. Goldman, E. A. Nagelhus and M. Nedergaard, *Sci. Transl. Med.*, 2012, **4**, 147ra111–147ra141.
135 A. Aspelund, S. Antila, S. T. Proulx, T. V. Karlsen, S. Karaman, M. Detmar, H. Wiig and K. Alitalo, *J. Exp. Med.*, 2015, **212**, 991–999.
136 A. Louveau, I. Smirnov, T. J. Keyes, J. D. Eccles, S. J. Rouhani, J. D. Peske, N. C. Derecki, D. Castle, J. W. Mandell, K. S. Lee, T. H. Harris and J. Kipnis, *Nature*, 2015, **523**, 337–341.
137 P. A. Soden, A. R. Henderson and E. Lee, *Adv. Biol.*, 2022, **6**, 2200027.
138 A. R. Yslas, R. Park, N. Nishimura and E. Lee, *Lab Chip*, 2024, **24**, 3826–3839.
139 R. Park, Y. Peng, A. R. Yslas and E. Lee, *APL Bioeng.*, 2025, **9**, 026126.
140 P. N. Ingram, L. E. Hind, J. A. Jiminez-Torres, A. Huttenlocher and D. J. Beebe, *Adv. Healthcare Mater.*, 2018, **7**, 1700497.
141 M. P. White, A. J. Rufaihah, L. Liu, Y. T. Ghebremariam, K. N. Ivey, J. P. Cooke and D. Srivastava, *Stem Cells*, 2013, **31**, 92–103.
142 A. Trillhaase, M. Maertens, Z. Aherrahrou and J. Erdmann, *Stem Cell Rev. Rep.*, 2021, **17**, 1741–1753.
143 C. M. Abreu, A. C. Lima, N. M. Neves, S. C. Kundu, R. L. Reis and D. Caballero, *Adv. Mater. Technol.*, 2025, **10**, 2400883.

144 S. Zhang, Z. Wan and R. D. Kamm, *Lab Chip*, 2021, **21**, 473–488.
145 J. J. Tronolone, N. Mohamed, C. P. Chaftari, Y. Sun, T. Mathur and A. Jain, *Curr. Protoc.*, 2024, **4**, e70058.
146 Z. Li, D. Yu, C. Zhou, F. Wang, K. Lu, Y. Liu, J. Xu, L. Xuan and X. Wang, *Biomater. Transl.*, 2024, **5**, 21–32.
147 T. V. Petrova and G. Y. Koh, *J. Exp. Med.*, 2018, **215**, 35–49.
148 Y. Peng and E. Lee, *Adv. Biol.*, 2023, e2300077, DOI: 10.1002/adbi.202300077.
149 R. Lu, A. M. Kolarzyk, W. D. Stamer and E. Lee, *Nat. Cardiovasc. Res.*, 2025, **4**, 1066–1076.
150 S. R. Cook, A. G. Ball, A. Mohammad and R. R. Pompano, *Lab Chip*, 2025, **25**, 155–174.
151 K. G. Birmingham, M. J. O'Melia, S. Bordy, D. Reyes Aguilar, B. El-Reyas, G. Lesinski and S. N. Thomas, *iScience*, 2020, **23**, 101751.
152 G. Goyal, P. Prabhala, G. Mahajan, B. Bausk, T. Gilboa, L. Xie, Y. Zhai, R. Lazarovits, A. Mansour, M. S. Kim, A. Patil, D. Curran, J. M. Long, S. Sharma, A. Junaid, L. Cohen, T. C. Ferrante, O. Levy, R. Prantil-Baun, D. R. Walt and D. E. Ingber, *Adv. Sci.*, 2022, 2103241, DOI: 10.1002/advs.202103241.
153 J. J. Tronolone, T. Mathur, C. P. Chaftari and A. Jain, *Ann. Biomed. Eng.*, 2023, **51**, 1723–1737.
154 J. J. Tronolone, T. Mathur, C. P. Chaftari, Y. Sun and A. Jain, *Bioeng. Transl. Med.*, 2023, **8**, e10582.
155 T. Mathur, J. J. Tronolone and A. Jain, *PLoS One*, 2024, **19**, e0299160.
156 M. Kim, S. Choi, D.-H. Choi, J. Ahn, D. Lee, E. Song, H. S. Kim, M. Kim, S. Choi, S. Oh, M. Kim, S. Chung and P. J. Park, *NPG Asia Mater.*, 2024, **16**, 7.
157 X. Cao, R. Ashfaq, F. Cheng, S. Maharjan, J. Li, G. Ying, S. Hassan, H. Xiao, K. Yue and Y. S. Zhang, *Adv. Funct. Mater.*, 2019, **29**, 1807173.
158 K. A. Deo, A. Murali, J. J. Tronolone, C. Mandrona, H. P. Lee, S. Rajput, S. E. Hargett, A. Selahi, Y. Sun, D. L. Alge, A. Jain and A. K. Gaharwar, *Adv. Healthcare Mater.*, 2024, **13**, 2303810.
159 S. Sundaram, J. H. Lee, I. M. Bjørge, C. Michas, S. Kim, A. Lammers, J. F. Mano, J. Eyckmans, A. E. White and C. S. Chen, *Nature*, 2024, **636**, 361–367.
160 S. Cometta, D. W. Hutmacher and L. Chai, *Biomaterials*, 2024, **309**, 122578.